



# Vibration Analysis of Curvilinearly Stiffened Composite Panel Subjected to In-Plane Loads

Wei Zhao\* and Rakesh K. Kapania†

*Virginia Polytechnic Institute and State University, Blacksburg, Virginia 24061*

DOI: 10.2514/1.J055047

This paper presents an efficient finite element approach to study the prestressed vibration mode results of a curvilinearly stiffened composite panel subjected to various in-plane loads. The present method models the plate and the stiffener separately, which allows the stiffener element nodes to not coincide with the plate shell-element nodes. The stiffness and mass matrices of a stiffener are transformed to those of the plate through the displacement compatibility conditions at the plate-stiffener interface via finite element interpolation. Convergence and validation studies have been conducted to verify the present method in the finite element vibration analysis by using the examples from the existing literature. Prestressed vibration mode results are examined for a stiffened composite panel with arbitrarily shaped composite stiffeners in the presence of the in-plane normal and shear loads. Numerical results show the possible benefits of using curvilinear stiffeners to improve the vibration response by increasing both the fundamental frequency and the buckling load through changing the vibration and buckling mode shapes with a negligible or even no weight penalty. The stiffener depth ratio is found to increase both the fundamental frequency and the buckling load, but only up to a certain value. Any further increase in the stiffener depth ratio causes stiffener buckling before plate buckling, and it leads the free and prestressed vibration mode results to behave as the vibration mode results for a plate with simply supported boundary conditions along the stiffeners.

## Nomenclature

$A_s$	= stiffener cross-sectional area
$a$	= length of the composite panel
$B$	= displacement-strain matrix
$b$	= width of the composite panel
$b_s$	= width of the composite stiffener
$D$	= constitutive matrix giving stress resultant-strain relations
$d$	= unit moving direction vector of the control point for curvilinear stiffener
$d_p$	= panel displacements
$d_s$	= stiffener displacements described in a local coordinate system
$d_{sg}$	= stiffener displacements described in the global coordinate system
$e$	= eccentricity of the stiffener; $(1/2)(t_p + h_s)$
$GJ$	= stiffener torsional stiffness
$h_s$	= stiffener height
$I_n, I_b$	= stiffener second moment of area about the $n$ and $b$ axes, respectively
$J$	= Jacobian of the coordinate transformation
$K$	= shear correction factor; equal to 5/6
$K_{Gp}$	= panel geometric stiffness matrix
$K_{Gs}$	= stiffener geometric stiffness matrix
$K_p$	= panel elastic stiffness matrix
$K_s$	= stiffener elastic stiffness matrix
$M_p$	= panel mass matrix
$M_s$	= stiffener mass matrix

$N_{cr}$	= critical buckling load for the stiffened laminated plate, N/mm
$N_{cr,p}$	= critical buckling load for the unstiffened cross-ply laminated plate, N/mm
$N_{sp}$	= shape functions to represent stiffener beam-element nodal displacement using panel shell-element nodal displacements
$N_{xx}, N_{yy}, N_{xy}$	= two in-plane normal loads and the in-plane shear load, respectively, N/mm
$R$	= radius of curvature of the curved stiffener
$T_s$	= transformation matrix
$t_p$	= panel thickness
$\alpha$	= angle between the stiffener tangential direction $t$ and the global $x$ axis
$\Gamma$	= stiffener arch length domain
$\Delta\epsilon$	= parameter for the stiffener placement
$\kappa$	= parameter for the stiffener geometric curvature
$\xi, \eta$	= natural coordinates
$\rho$	= material density
$\sigma^0$	= external in-plane stress vector
$\Omega$	= panel area domain
$\omega_1$	= first mode natural frequency for the stiffened composite plate, rad/s
$\omega_{1,p}$	= first mode natural frequency for the unstiffened cross-ply laminated plate, rad/s

## I. Introduction

COMPOSITE materials have been extensively used in fuselage and wing designs of aircraft structures, and they have demonstrated significant performance benefits due to their high specific stiffness-to-weight ratio and high strength-to-weight ratio [1,2]. Recent advances in manufacturing technologies, such as using the NASA Integrated Structural Assembly of Advanced Composites robot for rapid prototyping, and using vacuum assisted resin transfer molding, Pi-joining [2] and the pultruded rod stitched efficient unitized structure concept [3] for unitized stiffened composite plate, etc., have made it possible to build complex composite structures. These structures can be used for the unconventional aircraft configurations, for both lighter and more environment-friendly aircraft designs. These innovative manufacturing technologies require efforts toward developing new efficient analyses and design tools for the stiffened composite panels built using these new technologies.

Presented as Paper 2016-1500 at the 57th AIAA/ASCE/AHS/ASC Structures, Structural Dynamics, and Materials Conference, San Diego, CA, 4–8 January 2016; received 20 January 2016; revision received 1 August 2016; accepted for publication 2 August 2016; published online 18 October 2016. Copyright © 2016 by the authors. Published by the American Institute of Aeronautics and Astronautics, Inc., with permission. All requests for copying and permission to reprint should be submitted to CCC at www.copyright.com; employ the ISSN 0001-1452 (print) or 1533-385X (online) to initiate your request. See also AIAA Rights and Permissions www.aiaa.org/randp.

\*Graduate Research Assistant, Aerospace and Ocean Engineering; weizhao@vt.edu. Member AIAA.

†Mitchell Professor, Aerospace and Ocean Engineering; rkapania@vt.edu. Associate Fellow AIAA.

Curvilinear stiffeners/spars/ribs in the aircraft design were found to provide an enhanced design space for wing designs that would result in improved structural performance, as well as in reducing the structural weight because of their geometric curvature in addition to the placement and orientation [4–7]. The enhanced performance of these designs for an aircraft could lead to complex load distributions in the aircraft wing/fuselage panels due to their complex shaped geometry. These complex stress distributions could weaken or stiffen the panels, depending on the applied stress conditions. Local panel buckling, an increase in the local vibration amplitude, or panel flutter could occur when the applied in-plane stresses caused a large reduction in the panel transverse stiffness.

A structural analysis of composite plates received considerable research interest during the last few decades. Kapania and Raciti [8] gave a detailed summary of various shear-deformable theories for laminated plates and their suitability for structural analyses. Zhang and Yang [9] presented a detailed review of the finite element, free vibration, and dynamic analysis of composite laminated plates. Reddy and Khdeir [10] studied buckling and vibration responses of composite laminated plates using various plate theories, including the classical first- and third-order laminate theories. Carrera et al. [11] studied the vibration of a thin composite plate subjected to various in-plane loads by using the Carrera unified formulation and the finite element approach.

Stiffened composite structures have been widely used in many engineering applications to improve the vibration response while reducing the overall panel weight. Lee and Lee [12] studied the effects of the fiber ply orientation, the dimension, and the location of the stiffeners on the free vibration mode results of stiffened anisotropic plates by using the first-order shear-deformation theory. Rikards et al. [13] used an equivalent layer shell theory to study the buckling and vibration responses of laminated composite stiffened shells. Patel et al. [14] investigated the static and dynamic instability characteristics of stiffened shells subjected to uniform in-plane harmonic edge loading by using a finite element approach.

To obviate the need for imposing the stiffener element nodes to coincide with the plate shell-element nodes when there is a change in the stiffener shape, efforts have been made toward modeling the stiffeners and plates separately for a stiffened plate when using isoparametric elements in the finite element analysis. Mukherjee and Mukhopadhyay [15] used isoparametric shell elements for the free vibration analysis of the eccentrically stiffened plates. The stiffener displacement and geometry were expressed in terms of those of the plates through the displacement compatibility condition that makes use of interpolation functions in the finite element method. Therefore, the stiffeners could be placed anywhere within the plate element and not necessarily along the plate nodal lines. Ghosh and Biswal [16,17] used a four-node rectangular element for both the plate and the stiffeners. The stiffener element stiffness was reflected at all four nodes of the plate element in which the stiffener element node was located. Kumar and Mukhopadhyay [18] used a beam to model the stiffener for a stiffened laminated plate. The displacement and geometry of the stiffener beam-element nodes were interpolated by the nodes for the plate shell-element where the stiffener beam-element node was located. Later, this model was used by many researchers for a stiffened isotropic plate/shell and a stiffened laminated plate in static analysis [19], buckling analysis [20–22], free vibration, and transient dynamic analysis [23–26].

The increasing application of the integrated, bonded, and stitched stiffened composite structures for an aircraft wing/fuselage panel design along with the possible performance benefits of using arbitrarily shaped stiffeners could improve the structural prestressed vibration response by increasing the modal frequencies and by tailoring the vibration mode shapes, as well as by increasing the buckling load in the presence of various in-plane loads. Along with the benefit of using the present method in avoiding a repeated meshing when there is a change in the stiffener shape, a process required in the stiffener shape optimization; this paper improves the capabilities in EBF3PanelOpt [6] to design stiffened composite panel with arbitrarily shaped stiffeners, which is a PATRAN- and NASTRAN-based design optimization framework originally

developed for curvilinearly stiffened isotropic plate design. The present method uses separate modelings for the plate and the stiffeners, which can help us to improve the design space for the stiffeners for the stiffened plate design in addition to the stiffener geometric dimensions. Also, the present method avoids an increase in the number of degrees of freedom for a grid stiffened plate or for a stiffened plate with arbitrarily shaped stiffeners, which are typically seen when performing a NASTRAN structural analysis of such plates. Because a refined mesh is required in the finite element analysis when using NASTRAN, we need to guarantee the stiffener element nodes coincidence with the plate shell-element nodes.

The remainder of this paper is organized as follows: Sec. II mainly focuses on the mathematical formulations of appropriate finite elements for the vibration analysis of curvilinearly stiffened composite panels in the presence of the in-plane loads, and it shows the transformation of the stiffener's stiffness and mass matrices to be added to those for the plate. Section III.A presents results for convergence and validation studies by using the published results in the existing literature and those obtained by using MSC.NASTRAN. Section III.B shows the geometry parameterization approach for the stiffener shape in the stiffener placement and the stiffener geometric curvature for a curvilinear stiffener. Sections III.C and III.D, respectively, study the influence of the laminate configuration, the stiffener shape, and the stiffener depth ratio on the panel's free vibration response and the panel's prestressed vibration response subjected to in-plane biaxial and shear loads.

## II. Mathematical Formulation

### A. Strain Energy $U$ , Kinetic Energy $T$ , and Potential Energy $W$

Consider a curvilinearly stiffened panel as shown in Fig. 1a. The panel middle plane  $Oxy$  is chosen as the reference plane of the global coordinate system. The composite panel has the length, width, and thickness denoted as  $a$ ,  $b$ , and  $t_p$ , respectively. The strain energy  $U_p$  for the composite panel is

$$U_p = \frac{1}{2} \iint_{\Omega} \mathbf{d}_p^T B_p^T D_p B_p \mathbf{d}_p \, d\Omega \quad (1)$$

where  $\mathbf{d}_p$  is the generalized displacement field for the point at the middle surface of the composite panel. The displacement-strain matrix  $B_p$  used to describe the kinematic relation is given in Appendix A. The constitutive matrix  $D_p$  in the stress-strain relation can be found in [27].

The potential  $W_p$  of the panel due to the in-plane stress  $\sigma^0$  is

$$W_p = - \iiint_V (\sigma^0)^T \boldsymbol{\epsilon}_p^{\text{NL}} \, dV = - \frac{1}{2} \iint_{\Omega} \mathbf{d}_p^T (B_p^{\text{NL}})^T \boldsymbol{\sigma}_p B_p^{\text{NL}} \mathbf{d}_p \, d\Omega \quad (2)$$

where  $\boldsymbol{\epsilon}_p^{\text{NL}}$  is a vector for the nonlinear terms of the in-plane strains obtained through a Green–Lagrange strain tensor. The in-plane stress vector  $\boldsymbol{\sigma}^0$  among the panel can be obtained from residual stress, external applied load, initial displacement constraints, thermal stress, etc. The expressions for  $B_p^{\text{NL}}$  and  $\boldsymbol{\sigma}_p$  are given in Appendix A.

The kinetic energy  $T_p$  of the composite panel is

$$T_p = \frac{1}{2} \iint_{\Omega} \dot{\mathbf{d}}_p^T m_p \dot{\mathbf{d}}_p \, d\Omega \quad (3)$$

and  $m_p$  is given in Appendix A. The overdot represents the first-order derivative with respect to time.

Consider a curved blade stiffener as shown in Fig. 1b. The stiffener is attached arbitrarily to the plate with its laminate layers perpendicular to the panel middle plane. The solid rectangular cross section of the stiffener has the width and height denoted as  $b_s$  and  $h_s$ , respectively. The stiffener eccentricity  $e$  is defined as a measure of the offset between the stiffener neutral line and the panel middle plane:  $e = (1/2)(h_s + t_p)$ . When the stiffener neutral line coincides with the panel middle plane ( $e = 0$ ), we call the plate a concentrically stiffened panel. The warping of the stiffener is ignored in this study because the stiffener motion is governed by the plate. A local

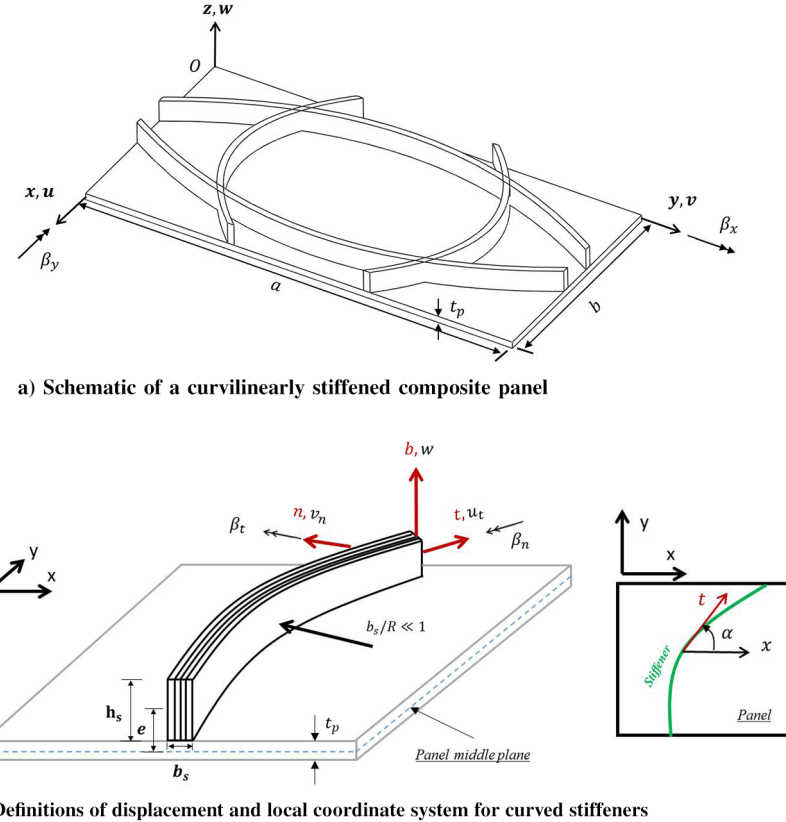


Fig. 1 Curvilinearly stiffened composite panel.

curvilinear coordinate system  $tnb$  is used to describe the motion of the curved stiffener, as shown in Fig. 1b. The stiffener is modeled as a three-dimensional (3-D) composite curved beam based on the Timoshenko beam theory.

For composite beam elements described in the local coordinate system  $tnb$ , all stresses can be neglected except the axial stress  $\sigma_{tt}$  and the shear stresses  $\tau_{tn}$  and  $\tau_{tb}$ . The strain components corresponding to those negligible stresses are not zeros. The strain energy  $U_s$  of the composite stiffener can be expressed as

$$U_s = \frac{1}{2} \int_{\Gamma} \boldsymbol{\epsilon}_s^T D_s^T \boldsymbol{\epsilon}_s d\Gamma = \frac{1}{2} \int_{\Gamma} \mathbf{d}_{sg}^T T_s^T B_s^T D_s B_s T_s \mathbf{d}_{sg} d\Gamma \quad (4)$$

where  $\Gamma$  is used to describe the stiffener length domain;  $T_s$  is a transformation matrix that relates the stiffener displacement field  $\mathbf{d}_s$  described in the local coordinate system  $tnb$  and the stiffener displacement field  $\mathbf{d}_{sg}$  described in the global coordinate system  $xyz$  ( $\mathbf{d}_s = T_s \mathbf{d}_{sg}$ );  $B_s$  is the stiffener displacement-strain matrix; and  $D_s$  is the stress resultants-strain constitutive matrix for the composite stiffener which has layers perpendicular to the panel middle plane. Expressions for  $B_s$ ,  $D_s$ , and  $T_s$  are given in Appendix B.

The potential energy for the stiffener  $W_s$  subjected to axial stress  $\sigma_{tt}$  can be expressed as

$$W_s = -\frac{1}{2} \int_{\Gamma} \mathbf{d}_{sg}^T T_s^T (B_s^{\text{NL}})^T \boldsymbol{\sigma}_s B_s^{\text{NL}} T_s \mathbf{d}_{sg} d\Gamma \quad (5)$$

where  $\boldsymbol{\sigma}_s$  is the axial stress matrix; the expressions for  $\boldsymbol{\sigma}_s$  and  $B_s^{\text{NL}}$  are given in Appendix B.

The kinetic energy for the stiffener  $T_s$  is

$$T_s = \frac{1}{2} \int_{\Gamma} \dot{\mathbf{d}}_{sg}^T T_s^T m_s T_s \dot{\mathbf{d}}_{sg} d\Gamma \quad (6)$$

where  $m_s$  is the stiffener mass matrix, which is given in Appendix B.

## B. Weak Form of Governing Equations

The finite element approach is employed to solve for the vibration response of the stiffened composite panel in the presence of both the in-plane normal loads and the in-plane shear load. Isoparametric eight-node shell elements and isoparametric three-node quadratic beam elements are used to approximate the composite panel and the stiffeners, respectively. The stiffener geometry and displacement fields are expressed in terms of those of the panel middle surface through finite element interpolation. As a result, the stiffener stiffness and mass matrices are transformed to those of the panel. Such a representation allows one to change the stiffener shape arbitrarily without changing the plate mesh in the finite element analysis.

The stiffener displacement  $\mathbf{d}_{sg}$  and geometry [ $\mathbf{r}_s = (x_s, y_s)$ ] described in the global coordinate system are approximated as

$$\mathbf{d}_{sg} = \sum_{i=1}^3 N_{s,i} d_{sg,i}, \quad \mathbf{r}_s = \sum_{i=1}^3 N_{s,i} \mathbf{r}_{s,i} \quad (7)$$

where  $N_{s,i}$  is the shape function for the three-node quadratic beam element; and the subscript  $i$  represents the  $i$ th node for the three-node beam element ( $i = 1, 2$ , and  $3$ ).

The displacement and geometry of the node for the three-node quadratic beam elements  $d_{sg,i}$  and  $r_{s,i}$  can be approximated by those of the nodes for the eight-node shell elements in which a beam-element node is located, as shown in Fig. 2. So, we have the displacement and geometry for the  $i$ th node of the three-node quadratic beam element expressed as

$$d_{sg,i} = \sum_{j=1}^8 N_{p,j} d_{p,j}, \quad r_{s,i} = \sum_{j=1}^8 N_{p,j} r_{p,j} \quad (8)$$

where  $N_{p,j}$  is the shape function of the eight-node shell element for the composite panel; and the subscript  $j$  represents the  $j$ th node for the eight-node shell element ( $j = 1, 2, \dots, 8$ ). Also,  $d_{p,j}$  and  $r_{p,j}$  are the shell-element nodal displacement and geometry, respectively. Here,  $r_{s,i}$  and  $r_{p,j}$  are the known coordinates of the stiffener and the

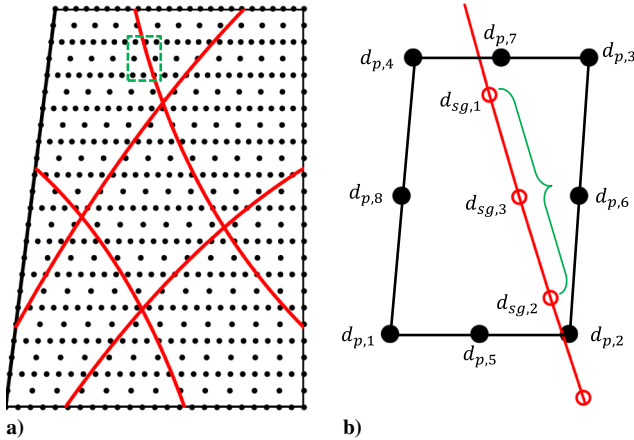


Fig. 2 Finite element mesh of the stiffened plate with arbitrarily shaped stiffeners.

plate element nodes, respectively. The natural coordinates  $\eta$  and  $\xi$  used in the plate shape function  $N_{p,j}$  for each stiffener element node are obtained from the geometry approximation. An inverse analysis is conducted to calculate the values for the natural coordinates  $\eta$  and  $\xi$  through the physical coordinates.

Substituting Eq. (8) into Eq. (7), we have

$$\mathbf{d}_{sg} = \sum_{i=1}^3 N_{s,i} \left( \sum_{j=1}^8 N_{p,j} d_{p,j} \right)_i, \quad \mathbf{r}_s = \sum_{i=1}^3 N_{s,i} \left( \sum_{j=1}^8 N_{p,j} r_{p,j} \right)_i \quad (9)$$

Write the geometry and displacement field of the stiffener in Eq. (9) in matrix form as

$$\mathbf{d}_{sg} = \mathbf{N}_{sp} \mathbf{d}_p, \quad \mathbf{r}_s = \mathbf{N}_{sp} \mathbf{r}_p \quad (10)$$

Equation (10) shows that the stiffener displacement and geometry for the approximated stiffener element nodes can be represented by those of the plate shell-element nodes. The stiffness and mass matrices for the stiffeners can hence be transformed to those for the panel.

Hamilton's principle is employed to obtain the weak form of the governing equation for vibration analysis of the curvilinearly stiffened composite panel subjected to in-plane loads, so we have the principle written as

$$\int_{t_1}^{t_2} \delta \mathbf{d}_p^T \left\{ \left[ \iint_{\Omega} \mathbf{B}_p^T \mathbf{D}_p^T \mathbf{B}_p d\Omega + \int_{\Gamma} \mathbf{N}_{sp}^T \mathbf{T}_s^T \mathbf{B}_s^T \mathbf{D}_s^T \mathbf{B}_s \mathbf{T}_s \mathbf{N}_{sp} \mathbf{d}_p d\Gamma \right] - \left[ \iint_{\Omega} (\mathbf{B}_p^{\text{NL}})^T \boldsymbol{\sigma}_p \mathbf{B}_p^{\text{NL}} d\Omega + \int_{\Gamma} \mathbf{N}_{sp}^T \mathbf{T}_s^T (\mathbf{B}_s^{\text{NL}})^T \boldsymbol{\sigma}_s \mathbf{B}_s^{\text{NL}} \mathbf{T}_s \mathbf{N}_{sp} \mathbf{d}_p d\Gamma \right] - \left[ \iint_{\Omega} m_p \ddot{\mathbf{d}}_p d\Omega + \int_{\Gamma} \mathbf{N}_{sp}^T \mathbf{T}_s^T m_s \mathbf{T}_s \mathbf{N}_{sp} \ddot{\mathbf{d}}_p d\Gamma \right] \right\} dt = 0 \quad (11)$$

Thus, we have the governing equations for free vibration analysis of the curvilinearly stiffened composite panel in the presence of the in-plane loads written as

$$[(K_p + K_s) - \lambda(K_{Gp} + K_{Gs}) - \omega^2(M_p + M_s)]\{\mathbf{d}_p\} = 0 \quad (12)$$

Here,  $K_p$  and  $K_s$  are the elastic matrices for the panel and the stiffeners, respectively;  $K_{Gp}$  and  $K_{Gs}$  are the differential stiffness matrices for the panel and the stiffeners due to the in-plane stresses, respectively;  $M_p$  and  $M_s$  are the mass matrices for the panel and the stiffeners, respectively; and  $\lambda$  is the in-plane load factor for which the value is less than the buckling load factor for linear prestressed modal analysis. Linear prestressed modal analysis means that the vibration analysis is conducted at the statically deformed equilibrium state of the stiffened plate. For the  $i$ th mode, the natural frequency  $\omega_i$  and the

corresponding mode shape  $\{\mathbf{d}_p\}_i$  can both be obtained by performing an eigenvalue analysis.

The element stiffness matrices  $K_p^e$  and  $K_s^e$ , the element differential stiffness matrices  $K_{Gp}^e$  and  $K_{Gs}^e$ , and the element mass matrices  $M_p^e$  and  $M_s^e$  for the curvilinearly stiffened composite panel, respectively, are

$$\begin{aligned} K_p^e &= \int_{-1}^{+1} \int_{-1}^{+1} \mathbf{B}_p^T \mathbf{D}_p^T \mathbf{B}_p \det \mathbf{J}_p d\xi d\eta \\ K_s^e &= \int_{-1}^{+1} \mathbf{N}_{sp}^T \mathbf{T}_s^T \mathbf{B}_s^T \mathbf{D}_s^T \mathbf{B}_s \mathbf{T}_s \mathbf{N}_{sp} \det \mathbf{J}_s d\xi \\ K_{Gp}^e &= \int_{-1}^{+1} \int_{-1}^{+1} (\mathbf{B}_p^{\text{NL}})^T \boldsymbol{\sigma}_p \mathbf{B}_p^{\text{NL}} \det \mathbf{J}_p d\xi d\eta \\ K_{Gs}^e &= \int_{-1}^{+1} \mathbf{N}_{sp}^T \mathbf{T}_s^T (\mathbf{B}_s^{\text{NL}})^T \boldsymbol{\sigma}_s \mathbf{B}_s^{\text{NL}} \mathbf{T}_s \mathbf{N}_{sp} \det \mathbf{J}_s d\xi \\ M_p^e &= \int_{-1}^{+1} \int_{-1}^{+1} m_p \det \mathbf{J}_p d\xi d\eta \\ M_s^e &= \int_{-1}^{+1} \mathbf{N}_{sp}^T \mathbf{T}_s^T m_s \mathbf{T}_s \mathbf{N}_{sp} \det \mathbf{J}_s d\xi \end{aligned} \quad (13)$$

where  $\mathbf{J}_p$  and  $\mathbf{J}_s$  are the Jacobians for the panel and the stiffener, respectively, and they are given in Appendix C.

The integration required for the stiffness and mass matrices calculations for the composite panel and the composite stiffeners are computed by using Gaussian quadrature rules. A selective integration technique is considered for the plate's stiffness and mass integrals. A  $3 \times 3$  full integration is employed for bending and mass integrals, and a  $2 \times 2$  reduced quadrature is employed for computing other stiffness integrals. For the three-node curved beam element, reduced integration with two Gaussian points is considered for all stiffness and mass integrals [28].

### III. Results and Discussions

#### A. Convergence and Validation

##### 1. Free Vibration Analysis of Curvilinearly Stiffened Isotropic Panels

A simply supported rectangular isotropic panel with two different eccentric curved stiffeners, used by Tamijani and Kapania [29], is considered in this section to verify the program for studying free vibration analysis. The plate has a length and width of 606.9 and 711.2 mm, respectively. The geometry dimensions of the plate and the stiffener cross section are shown in Fig. 3. Both the plate and the stiffeners are made of the same isotropic material with a Young's modulus of  $E = 73$  GPa, a Poisson's ratio of  $\nu = 0.33$ , and a material density of  $\rho = 2837$  kg/m<sup>3</sup>. A convergence study on the modal frequencies with respect to the element size for the stiffened panel is conducted, and the results are shown in Table 1. It is seen that converged results can be obtained by using a  $12 \times 12$  mesh for the panel and 15 beam elements for each stiffener in the present analysis.

Table 2 shows a comparison of the natural frequencies obtained from the present method, NASTRAN, and other literature for a plate with two different-shaped stiffeners. For both cases, a refined mesh in the NASTRAN model is considered to ensure the converged results are used for validation. There are 2532 triangular shell elements and 43 beam elements used in the NASTRAN model for the plate and stiffener 1, respectively. For the plate with stiffener 2, there are 2522 triangular shell elements and 48 beam elements. Natural frequencies and the corresponding mode shapes of the first six modes obtained from the present method compare well with other results as shown in Table 2 and Fig. 4, respectively, for both cases. The mode shapes in the literature [29] are not shown here because there are only two vibration mode shapes (mode 5 and mode 10) for the stiffened plate with stiffener 1. The free vibration mode shapes of modes 5 and 10 for the stiffened plate with stiffener 1 obtained from the present method also compare well with those in the literature [29].

The present method, in terms of the CPU time, is more efficient than using PATRAN/NASTRAN in geometry and mesh generation and eigenvalue computations, which is a process required for shape optimization. The CPU time for PATRAN/NASTRAN refers to the

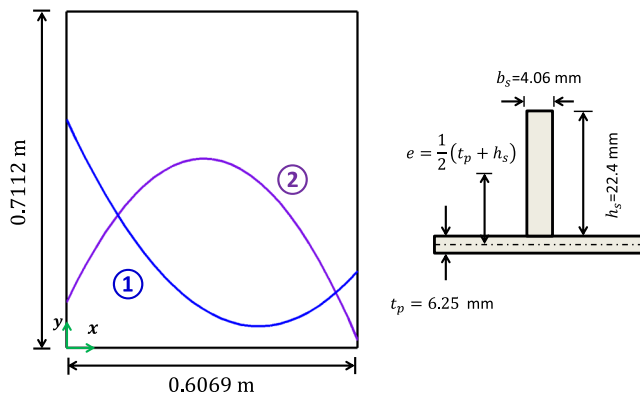


Fig. 3 Geometry of curvilinearly stiffened plate and stiffener cross section. The two stiffeners curve functions are 1)  $y = 1.2(0.6 - 1.5x)^2 + 0.05$ ; and 2)  $y = -30(0.1 - 0.35x)^2 + 0.4$ .

one taken by EBF3PanelOpt [6], as EBF3PanelOpt uses PATRAN and NASTRAN for geometry and mesh generation, as well as eigenvalue computations. For a stiffened plate with a lot of stiffeners, the present method can calculate the natural coordinates for the element nodes of each stiffener in parallel through a multiprocessor computation.

## 2. Free Vibration Analysis of Stiffened Composite Panel

A fully clamped composite panel stiffened by one straight longitudinal stiffener along the panel length direction is employed to verify the present method for free vibration analysis of stiffened composite panels. The nominal ply mechanical properties for the composite material of AS1/3501-6 that is used are given by  $E_1 = 128$  GPa,  $E_2 = 11$  GPa,  $G_{12} = G_{13} = 4.48$  GPa,

$G_{23} = 1.53$  GPa,  $\nu_{12} = 0.25$ , and the density of  $\rho = 1500$  kg/m<sup>3</sup>. The layer stacking sequence for the skin plate is  $[0/\pm 45/90]_s$ . Each laminate layer has a thickness of 0.13 mm, and the stiffener has a layer stacking sequence, throughout the stiffener thickness, of  $[0_7/90_7]_s$ . Here, a  $12 \times 12$  mesh for the panel and 15 beam elements for the stiffener are used for this model. The natural frequencies of the stiffened composite panel with a straight composite stiffener obtained from the present method compare well with the available results [12,13], as seen in Table 3.

## B. Geometry Parameterization for Stiffener Shape

To quantify the change in the mode results with the stiffener shape, a previously developed geometry parameterization tool is used to parameterize the stiffener shape for a curvilinearly stiffened composite panel. The placements of the start and end points (points A and B) for each stiffener are parameterized by perimeter parameters  $\epsilon_A$  and  $\epsilon_B$  in the parametric space (Fig. 5a). The natural coordinates  $\xi$  and  $\eta$  for points A and B in the natural space can be obtained from the relations tabulated in Table 4. The middle point is a control point that governs the stiffener shape, which is assumed to move from the initial position  $x_0(\epsilon) = (\xi_0(\epsilon), \eta_0(\epsilon))$  in direction  $d$  with a parameter for the geometric curvature  $\kappa$  to the current position,  $x(\epsilon, \kappa) = (\xi(\epsilon, \kappa), \eta(\epsilon, \kappa))$  (Fig. 5b). The expression for the natural coordinates  $x$  for the control points can be written as

$$x(\epsilon, \kappa) = x_0(\epsilon) + D_c \kappa \quad (14)$$

$D_c$  is a matrix for the moving directions  $d$  for all control points. Additionally,  $d$  is a unit normal vector to the vector from the start point to the end point. The initial control point position  $x_0$  is obtained by averaging the natural coordinates of the start and end points. The B-spline approach is used to generate the stiffener curve using the

Table 1 Convergence study of stiffened panel free vibration modal frequency (in hertz) with element mesh size: stiffener 1<sup>a</sup>

Mode no.	Mesh size					
	$4 \times 4$ (5) <sup>a</sup>	$8 \times 8$ (10)	$12 \times 12$ (15)	$16 \times 16$ (20)	$20 \times 20$ (30)	$24 \times 24$ (40)
1	88.2	86.6	86.4	86.3	86.3	86.2
2	194.8	187.1	186.5	186.3	186.1	186.1
3	229.9	217.2	216.4	216.1	215.9	215.9
4	362.5	319.4	317.7	317.3	317.2	317.1
5	407.2	358.3	355.4	354.7	354.1	351.0
6	476.2	424.6	422.0	421.4	421.2	421.1
7	670.8	493.4	488.3	487.6	487.4	487.3
8	728.8	553.4	545.7	544.4	543.5	543.3
9	766.4	586.4	577.9	576.1	575.2	575.0
10	890.4	679.5	665.6	664.0	663.6	663.6

<sup>a</sup>The values in the parentheses are the numbers for each stiffener beam element.

Table 2 Natural frequencies (in hertz) of a curvilinearly stiffened plate with a different-shaped stiffener

Mode	Stiffener 1				Stiffener 2			
	ANSYS [29]	Mesh free [29]	NASTRAN	Present	ANSYS [29]	Mesh free [29]	NASTRAN	Present
1	84	83	85.9	86.4	83	85	83.9	85.1
2	183	175	185.0	186.5	190	184	190.2	191.9
3	213	217	215.1	216.4	229	241	228.1	230.9
4	316	319	315.9	317.7	316	314	316.9	319.0
5	347	327	351.0	355.4	331	327	331.8	334.0
6	417	421	420.0	422.0	454	457	456.6	463.3
7	485	489	485.6	488.3	485	500	485.5	490.9
8	536	521	539.3	545.7	538	526	535.9	542.8
9	567	561	569.8	577.9	558	561	559.3	563.4
10	662	661	663.2	665.6	688	680	692.1	698.8
CPU Time <sup>a</sup>	—	—	2.3	1.1	—	—	2.1	1.0

<sup>a</sup>The normalized time is considered here because the CPU times are different for different machines (CPU time refers to the total time used for geometry parameterization, mesh generation, and eigenvalue computation).

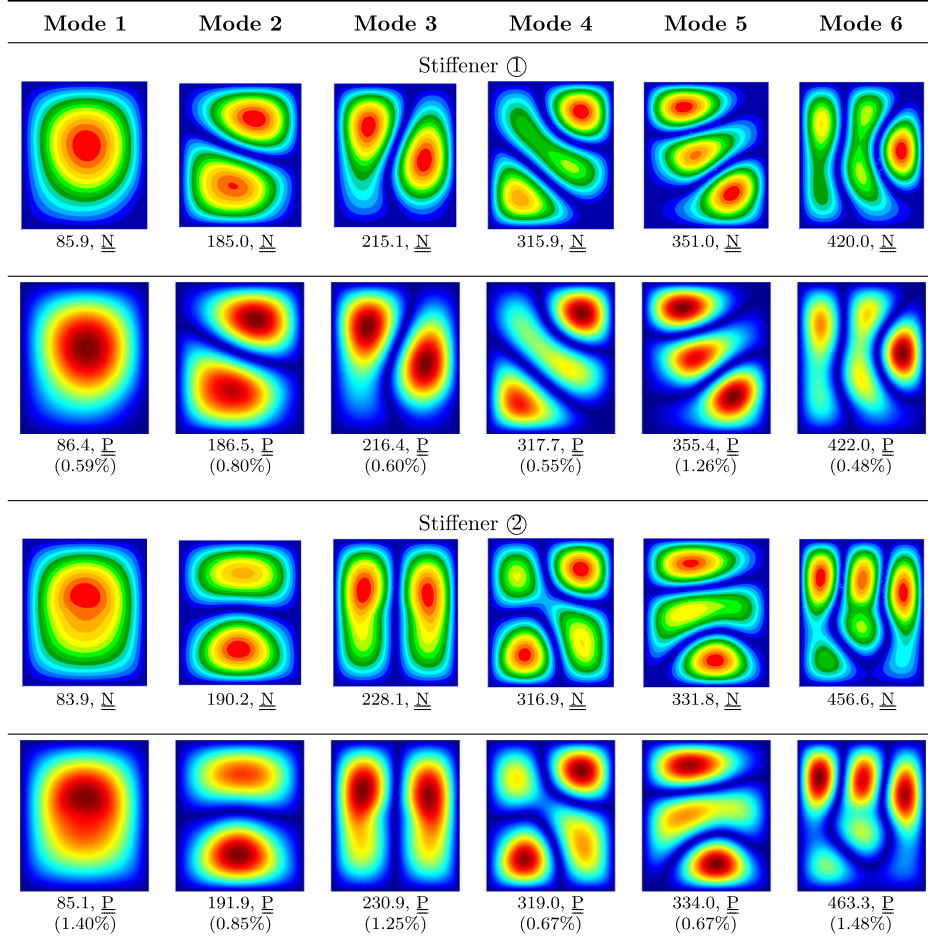


**Fig. 4 Comparisons of free vibration mode results obtained from NASTRAN and the present method; N denotes NASTRAN, and P denotes the present analysis.**

three points: points A and B, and the control point in the natural space. The isoparametric shape functions for the four-node quadrilateral element in the finite element method are then used as mapping functions to transform the stiffeners defined in the natural space to the physical space. One can use this parameterization tool to generate the stiffener for both a curvilinearly stiffened plate and a grid stiffened plate, as shown in Figs. 5c and 5d, respectively. Therefore, the parameters for a curvilinear stiffener include the stiffener placements,  $\epsilon = \{\epsilon^A, \epsilon^B\}$ , and the stiffener geometric curvature  $\kappa$ . A detailed description for the stiffener geometric parameterization can be found in the work of Zhao and Kapania [22]. This work focuses on studying the free and prestressed vibration response of a curvilinearly stiffened composite panel for different stiffener placements  $\epsilon$  and different stiffener geometric curvatures  $\kappa$ .

### C. Free Vibration Analysis of Curvilinearly Stiffened Composite Panel

A simply supported square composite panel with dimensions of  $800 \times 800$  mm is considered in this study. The panel thickness-

to-width ratio is assumed to be 0.01. The width of the stiffener is the same as the panel thickness:  $b_s = t_p$ . The materials for both the panel and the stiffeners are T300/5208 graphite/epoxy composites, for which the material properties are tabulated in Table 5. The strong material direction coincides with the stiffener length direction. Eight-layer symmetric laminates are considered for both the stiffeners and the composite laminated plate. The convergence study of this model for a buckling load variation with a finite element size was examined in our previous paper [22]. A convergence study for the vibration analysis is conducted for this paper. To save space, the convergence study on the natural frequencies with the plate and stiffener mesh size is not shown here. A  $12 \times 12$  mesh for the panel and 15 beam elements for each stiffener are considered for this model in the following finite element vibration analysis. In the following examples, each stiffener is assumed to be attached eccentrically to the plate and the stiffener laminates are perpendicular to the panel middle plane unless otherwise specified.

The two stiffeners in the studied model as shown in Fig. 6 are symmetric about the panel center line:  $x = a/2$ . The start and end points for each curve are located on the top and bottom sides of the

**Table 3 Natural frequencies (in hertz) of a stiffened composite panel with a composite stiffener**

Mode	Unstiffened panel			Stiffened panel		
	Lee and Lee [12]	Rikards et al. [13]	Present	Lee and Lee [12]	Rikards et al. [13]	Present
1	85.1	85.6	85.1	213.8	215.0	214.8
2	134.0	135.7	134.3	229.4	235.5	228.7
3	207.4	208.1	206.9	270.2	274.5	273.1
4	216.1	219.9	216.7	313.8	315.4	313.6
5	252.5	256.3	253.1	354.0	361.4	358.4

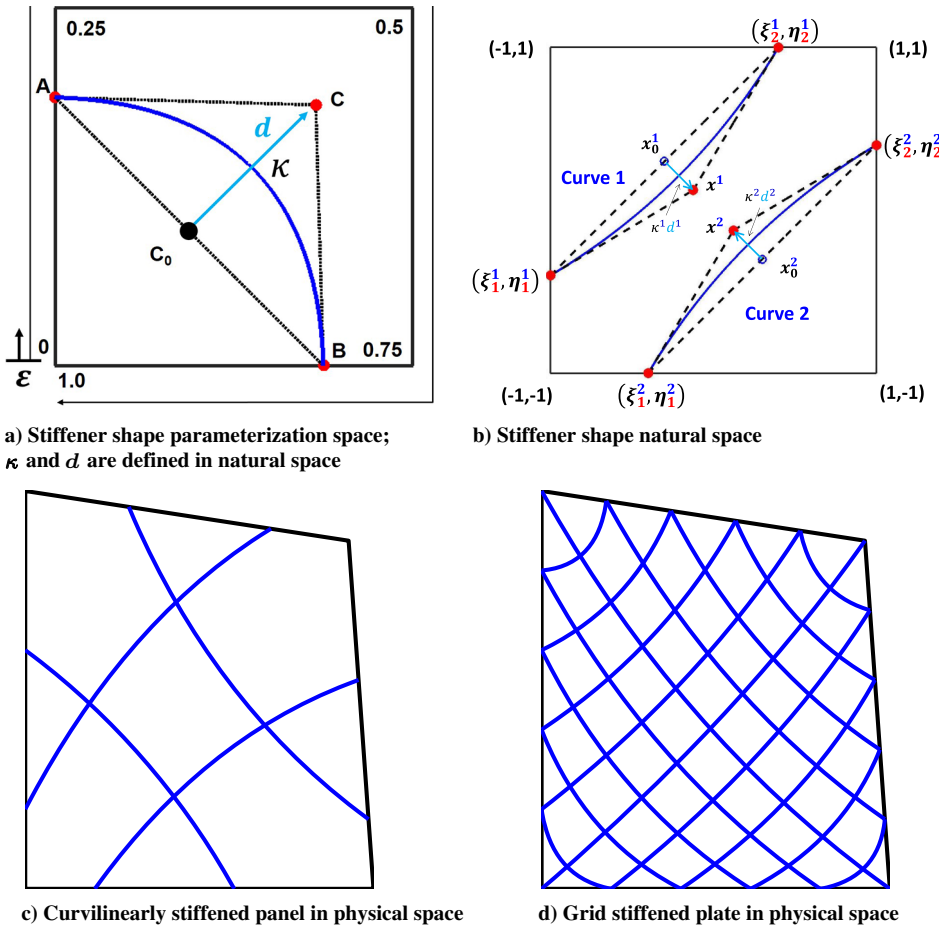


Fig. 5 Parameterization of the stiffener shape for curvilinearly stiffened plates.

natural space, respectively. In fact, the stiffeners can be located in any place within the plate by using the developed geometric parameterization tool. We select the two symmetric stiffeners to study the effect of the stiffener placement and the stiffener geometric curvature on the panel's vibration responses.

Table 4 Relationship between the perimeter parameter  $\epsilon$  and natural coordinates  $\xi$  and  $\eta$ 

$\epsilon$	$\xi$	$\eta$
$0 \leq \epsilon < 0.25$	-1	-1 + 8 $\epsilon$
$0.25 \leq \epsilon < 0.50$	$-1 + 8(\epsilon - 0.25)$	1
$0.50 \leq \epsilon < 0.75$	1	$-8(\epsilon - 0.5) + 1$
$0.75 \leq \epsilon \leq 1.00$	$-1 - 8(\epsilon - 1)$	-1

Table 5 Material properties of T300/5208 graphite/epoxy composite material

Parameter	Value
$E_1$	132.38 GPa ( $19.2 \times 10^6$ psi)
$E_2$	10.76 GPa ( $1.56 \times 10^6$ psi)
$E_3$	10.76 GPa ( $1.56 \times 10^6$ psi)
$G_{12} = G_{13}$	5.65 GPa ( $0.82 \times 10^6$ psi)
$G_{23}$	3.38 GPa ( $0.49 \times 10^6$ psi)
$\nu_{12} = \nu_{13}$	0.24
$\nu_{23}$	0.49
$\rho$	1800 kg/m <sup>3</sup> (0.065 lb/in. <sup>3</sup> )

### 1. Influence of Stiffener Geometric Curvature on Panel's Free Vibration Responses

The influence of the stiffener geometric curvature on the panel's fundamental frequency is studied first. For curve 1, the placement parameters of the start and end points are  $\epsilon^A = (0.25 + \Delta\epsilon^A)$  and  $\epsilon^B = (1 - \Delta\epsilon^B)$ , respectively.  $\Delta\epsilon^A = \Delta\epsilon^B = \Delta\epsilon = 0.0625$  is considered for stiffener curve 1 in this case. The stiffener depth ratio,  $h_s/b_s = 5$ , is used in this case for the free vibration analysis study.

Figure 7 shows the variation of the normalized fundamental frequency for the stiffened composite panel with the stiffener geometric curvature when the stiffener placements are fixed. For comparison, the normalized frequency is obtained with respect to the fundamental frequency of the unstiffened symmetrically cross-ply laminated plate  $\omega_{1,p}$ . The negative value of the geometric curvature means that the control point moves with the same magnitude but in the opposite direction with the moving direction vector  $d$ . The zero geometric curvature ( $\kappa = 0$ ) represents the straight stiffeners for the composite plate.

The 0 deg laminated stiffener is found to be much more effective in improving the plate's fundamental frequency. This is because a laminated composite stiffener with 0 deg fiber ply orientation provides the largest stiffness contribution to the plate's transverse stiffness.

The stiffener geometric curvature is found to influence the value of the fundamental frequency significantly for all the cases studied here. Among the four laminate configurations, the stiffened symmetrically cross-ply laminated plate with 0 deg laminated stiffeners is found to be the most effective in increasing the fundamental frequency. The variation of the fundamental frequencies with the stiffener geometric curvature for the four laminate configurations are almost similar. Take the stiffened cross-ply laminated plate with the 0 deg laminated

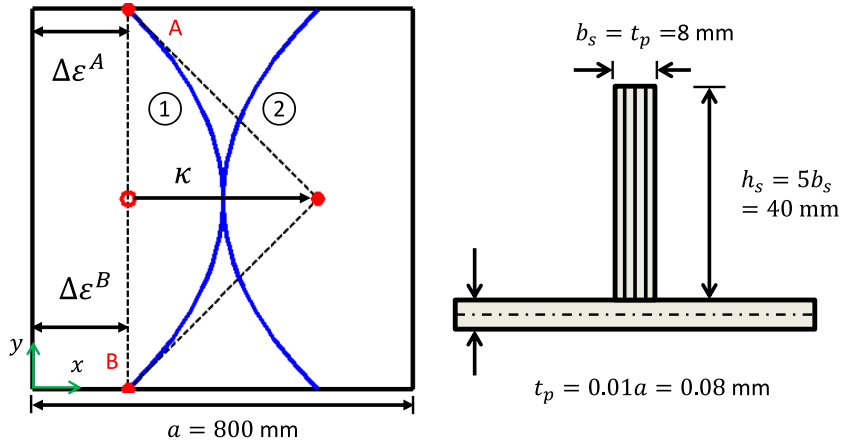


Fig. 6 Geometry and cross section of the curvilinearly stiffened plate;  $\Delta\epsilon^A = \Delta\epsilon^B = \Delta\epsilon$ .

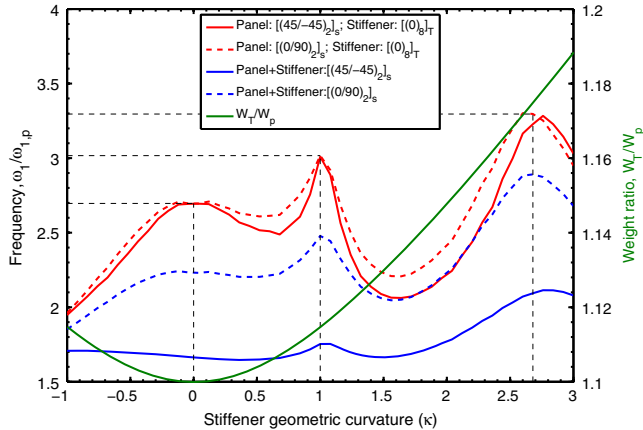


Fig. 7 Variation of the normalized fundamental frequency with the stiffener geometric curvature;  $\omega_{1,p} = 346.7$  rad/s.

stiffeners for an example. When compared to the fundamental frequency and weight for the plate with straight stiffeners ( $\kappa = 0$ ), the configuration with the stiffener geometric curvature  $\kappa = 1$  increases the plate fundamental frequency by almost 30% with a mere 1.5% panel weight increase. The configuration with the stiffener geometric curvature  $\kappa = 2.7$  increases the panel's fundamental frequency to the largest value by up to 60% but with a nearly 7.0% panel weight increase. This demonstrates the possible benefit of tailoring the stiffener shape to increase the fundamental frequency for a stiffened plate with a lower weight penalty.

The discontinuous change in the fundamental frequency with the stiffener geometric curvature is because of the change in the corresponding mode shape. Figure 8 shows the variation of the first bending mode shape for the stiffened composite plate for different stiffener geometric curvatures. It is clearly seen that the stiffener geometric curvature changes the first bending mode shape significantly, and hence leads to a discontinuous change in the frequency value with the stiffener geometric curvature.

## 2. Influence of Stiffener Placement on Panel's Free Vibration Responses

The parameter for the stiffener geometric curvature for stiffener 1 as shown in Fig. 6 is fixed as  $\kappa = 1$ ; the start and the end points move parallel to the  $x$  axis with the same value:  $\Delta\epsilon$ . Figure 9 shows the variation of the fundamental frequency with the stiffener placement for the four different laminate configurations. The stiffeners move parallel to the  $x$  axis; there is no change in the total weight of the curvilinearly stiffened composite panel. Therefore, there is a horizontal line to represent the change of the total weight with the stiffener placement. The stiffener depth ratio ( $h_s/b_s = 5$ ) is considered in this case for the free vibration analysis study.

It is clearly seen that the stiffener placement increases the fundamental frequency significantly without any weight penalty.

Like the most effective configuration in the case studied in the previous section, the curvilinearly stiffened cross-ply laminated plate with the 0 deg laminated stiffeners is the most effective design in increasing the fundamental frequency.

The variations of the normalized fundamental frequencies with the stiffener placements are similar for the four laminate configurations. Considering the stiffened cross-ply laminated plate with 0 deg laminated stiffeners, when comparing to the straight stiffener configuration in the previous section, the stiffened plate at the stiffener placement of  $\Delta\epsilon = 0.1388$  increases the fundamental frequency by around 60% to the largest value. This fundamental frequency increase is the same as the one for the case ( $\kappa = 2.7$  and  $\Delta\epsilon = 0.0625$ ) studied in the previous section. However, this configuration only has a 1.5% panel weight penalty as compared to that with a nearly 7% panel weight penalty in improving the fundamental frequency to the largest value. This demonstrates that further improvement in increasing the fundamental frequency with a lesser weight penalty can be achieved by changing the stiffener placement in addition to tailoring the stiffener geometric curvature.

As expected, the discontinuous change in the fundamental frequency with the stiffener placement is because of the change in the first vibration mode shape. The variations of the first vibration mode shape with the stiffener placements are shown in Fig. 10. It is clearly seen that the free vibration mode shapes for the fundamental frequency morph with the stiffener placement.

## 3. Influence of Stiffener Depth Ratio on Panel's Free Vibration Responses

The influence of the stiffener depth ratio  $h_s/b_s$  on the fundamental vibration mode results is examined in this case. The stiffener geometric curvature and the stiffener placement for stiffener 1, as shown in Fig. 6, are fixed as  $\kappa = 1$  and  $\Delta\epsilon = 0.1388$ , respectively.

A stiffener depth ratio of five is assumed in the previous two sections for the stiffener shape study. Figure 11 shows the variation of the fundamental frequency with a stiffener depth ratio up to 20 for all laminated configurations. It is clearly seen that increasing the stiffener depth ratio can further increase the value of the fundamental frequency for all laminated configurations.

Numerical results also show that there is one threshold value for the stiffener depth ratio for each configuration that leads to the highest value of the fundamental frequency. The fundamental frequency increases significantly with the stiffener depth ratio up to this threshold value. As the stiffener depth ratio increases further beyond this threshold value, the fundamental frequency starts to decrease slightly. This is because any further increase in the stiffener depth ratio increases the stiffener equivalent bending stiffness, which could cause the plate to behave as if it is simply supported along the stiffeners. The plate is divided into several subplates. The increase in the total mass due to the higher stiffener weight causes increases in both the mass and rotational inertias, which leads to a slight reduction in the fundamental frequency. For the same laminated plate with different laminated stiffeners, these near-simply supported boundary conditions due to the larger stiffener's equivalent bending stiffness

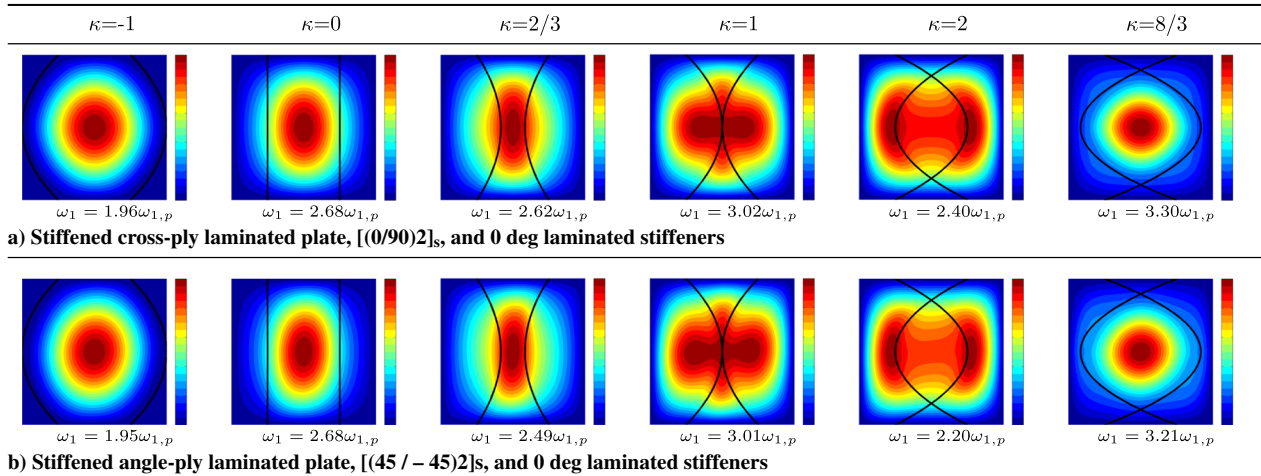


Fig. 8 Variation of the fundamental mode shape with the stiffener geometric curvature;  $\omega_{1,p} = 346.7$  rad/s.

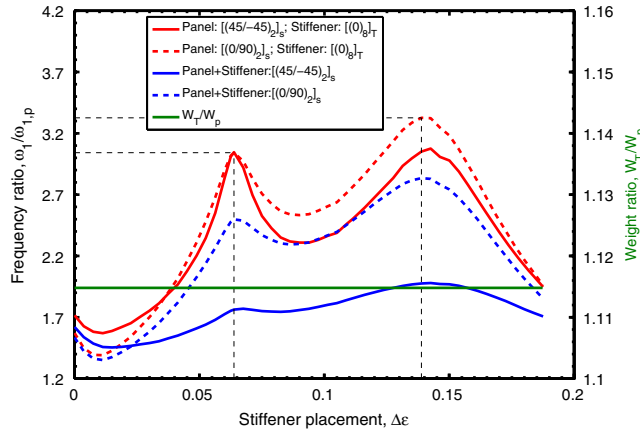


Fig. 9 Variation of the normalized fundamental frequency with the stiffener placement;  $\omega_{1,p} = 346.7$  rad/s.

cause the two curves of the frequency with the stiffener depth ratio to become close. The change in the first free vibration mode shape with the stiffener depth ratio is shown in Fig. 12. It is these near-simply supported boundary conditions that cause the first bending mode to vary from a global mode to a local mode.

Numerical results also show that, although the unstiffened angle-ply laminated plate is found to have a larger fundamental frequency than the unstiffened cross-ply laminated plate, the stiffened symmetrically cross-ply laminated plate is found to be more

effective in increasing the fundamental frequency than the stiffened symmetrically angle-ply laminated plate. It is believed that the specific stiffness from the studied stiffener shape and the 0 deg laminated configuration for the stiffeners increase the transverse stiffness for the cross-ply laminated plate to a larger value than that for the angle-ply laminated plate, which leads to a larger fundamental frequency for the stiffened cross-ply laminated plate.

#### D. Prestressed Vibration Analysis of Curvilinearly Stiffened Composite Panel

Previous work [22] and the preceding sections both show that the plate laminate configuration, the stiffener shape, and the stiffener depth ratio can increase the values for both the critical buckling load and the fundamental frequency with a low weight penalty. To further investigate the influence of the stiffener shape and the laminate configuration on the panel's prestressed vibration response, this section studies the fundamental frequency and the corresponding mode shape for a prestressed plate with different laminated configurations and different stiffener shapes. The thermal effect is not considered in the current study. The applied in-plane load is assumed to not cause the laminate fiber failure. In the following studies, the 0 deg laminated stiffener is only considered for the curvilinearly stiffened composite panel because it increases the panel's transverse stiffness with a lower weight penalty. The studied model is shown in Fig. 6, which is the same as the one used for the free vibration analysis in previous sections.

For comparison, the eigenvalues in the prestressed natural frequency and the buckling load shown in the following are normalized with

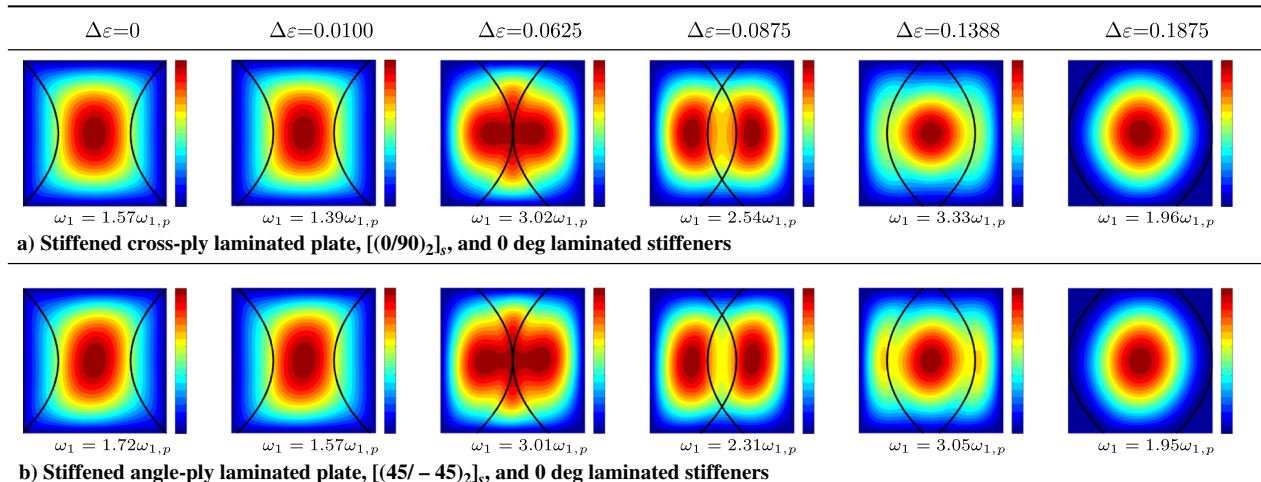


Fig. 10 Variation of the fundamental mode shape with the stiffener placement;  $\omega_{1,p} = 346.7$  rad/s.

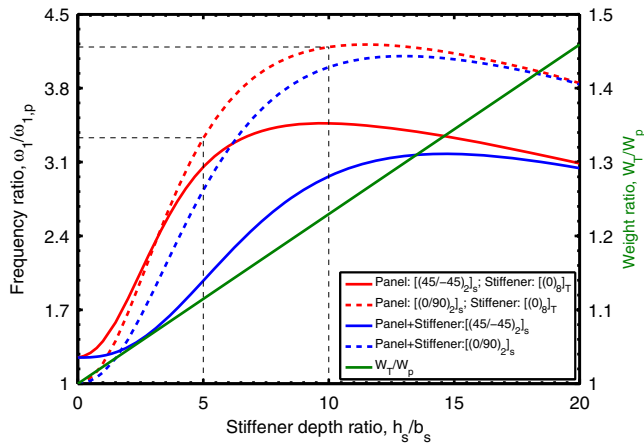


Fig. 11 Variation of the normalized fundamental frequency with the stiffener depth ratio;  $\omega_{1,p} = 346.7 \text{ rad/s}$ .

respect to those for the unstiffened cross-ply laminated plate. The free vibration frequency (in radians per second) and the critical buckling load (in newtons per millimeter) for the unstiffened cross-ply laminated plate are  $\omega_{1,p}$  and  $N_{cr,p}$ , respectively. The value for  $N_{cr,p}$  is different for different applied in-plane load conditions. There is one prestressed case considered for a stiffened laminated plate in the presence of an in-plane shear load  $N_{xy}$  because changing the shear load direction does not change the natural frequencies of the prestressed plate. The prestressed mode results are examined for the curvilinearly stiffened composite plate in the presence of the critical buckling load  $N_{cr,p}$  for the unstiffened cross-ply laminated plate. A positive value for the in-plane load implies a tensile load being applied at the panel edge; a negative value, a compressive load.

### 1. Influence of Stiffener Geometric Curvature on Panel's Prestressed Vibration Responses

Figure 13 shows the variation of the buckling load and the prestressed fundamental frequency with the stiffener geometric curvature for the stiffened composite panel in the presence of the in-plane biaxial loads  $N_{xx}$  and  $N_{yy}$  and the in-plane shear load  $N_{xy}$ . The stiffener placement for stiffener curve 1 is  $\Delta\epsilon = 0.0625$ . The stiffener depth ratio is assumed to be five in this study.

For both laminated configurations, numerical results show that the variations of the buckling load and the prestressed fundamental frequency with the geometric curvature are similar to each other. The geometric curvature values for the most effective design in increasing both the buckling load and the prestressed fundamental frequency are close to each other. This demonstrates the possible benefit of tailoring the stiffener geometric curvature to improve the prestressed vibration

response by increasing both the buckling load as well as the fundamental frequency simultaneously.

Like the most effective design of the cross-ply laminated plate with 0 deg laminated stiffeners in increasing the fundamental frequency in the previous free vibration analysis, it is also found that this laminated configuration is the most effective in increasing the buckling load. The specific stiffness from the stiffener shape studied in this case and the 0 deg laminated configuration for the stiffeners increases the elastic stiffness to a larger value for the cross-ply laminated plate than that for the angle-ply laminated plate. As expected, the fundamental frequency increases with the in-plane tensile loads and decreases with the in-plane compressive and shear loads. For the vibration response in the presence of the in-plane shear load, the variations of the fundamental frequency with the stiffener geometric curvature are almost same for the free vibration and prestressed vibration cases. This is because the geometric stiffness due to the shear load has less influence on the diagonal terms in the stiffness matrix, which leads to a lower influence on the eigenvalues, as compared to the in-plane normal loads.

Numerical results also show the discontinuous change of the two eigenvalues, the buckling load, and the fundamental frequency with the stiffener geometric curvature. To study this reason, the buckling mode shape and the prestressed vibration mode shape for the stiffened cross-ply laminated plate are examined, and they are shown in Figs. 14 and 15. It is clearly seen that both the buckling mode shape and the vibration mode shape change with the stiffener geometric curvature in the two different load conditions. This explains that the change in the mode shapes causes the discontinuous changes of the mode frequency and the buckling load with the stiffener geometric curvature.

### 2. Influence of Stiffener Placement on Panel's Prestressed Vibration Responses

Figure 16 shows the variation of the buckling load and the fundamental frequency with the stiffener placement  $\Delta\epsilon$  for the stiffened composite panel in the presence of the in-plane biaxial and shear loads. The stiffener geometric curvature for stiffener curve 1 is  $\kappa = 1$ . The stiffener depth ratio is assumed to be five in this case.

Numerical results for all four laminated configurations show that it is possible to change the stiffener placement to improve the prestressed vibration response by increasing both the critical buckling load and the fundamental frequency without any weight increase. Numerical results also show that the variations of the buckling load and the prestressed fundamental frequency with the stiffener placement are similar. The closeness in the values of the stiffener placements for the most effective stiffener configuration in simultaneously increasing both the buckling load and the fundamental frequency to the highest values demonstrates the possible benefit of tailoring the stiffener placement in improving the prestressed vibration response.

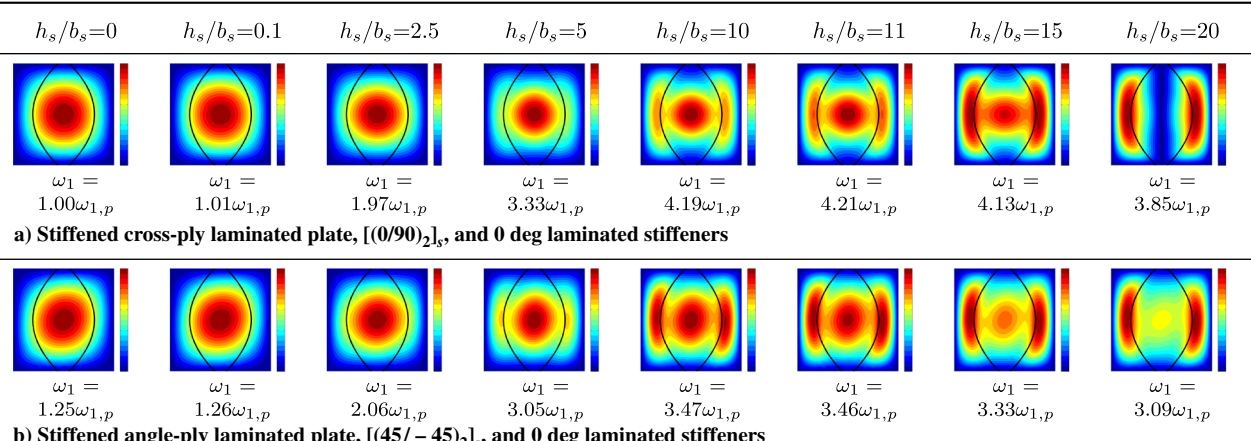


Fig. 12 Variation of the fundamental mode shape with the stiffener depth ratio;  $\omega_{1,p} = 346.7 \text{ rad/s}$ .

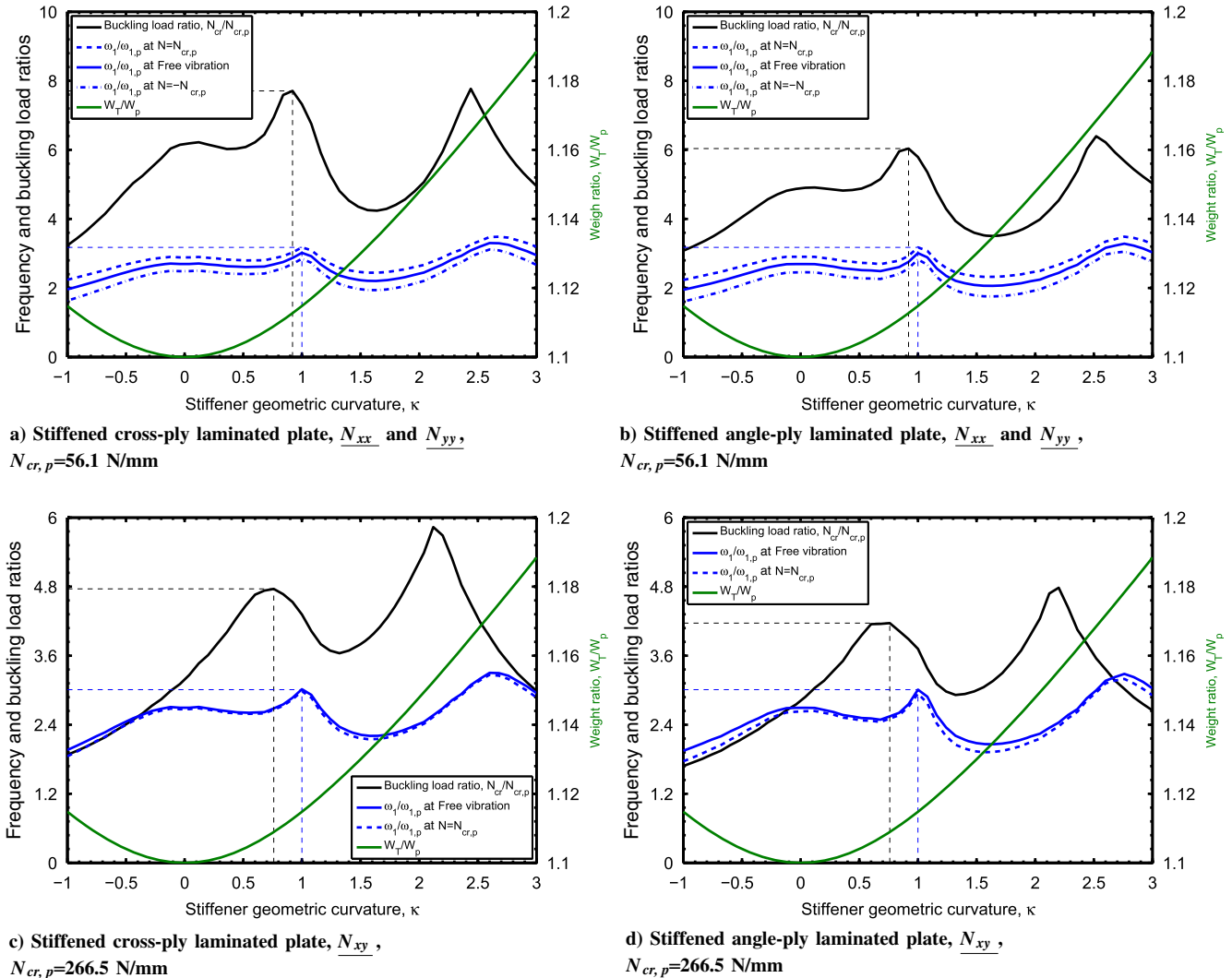


Fig. 13 Variation of the buckling load and the prestressed fundamental frequency with the stiffener geometric curvature;  $\omega_{1,p} = 346.7$  rad/s.

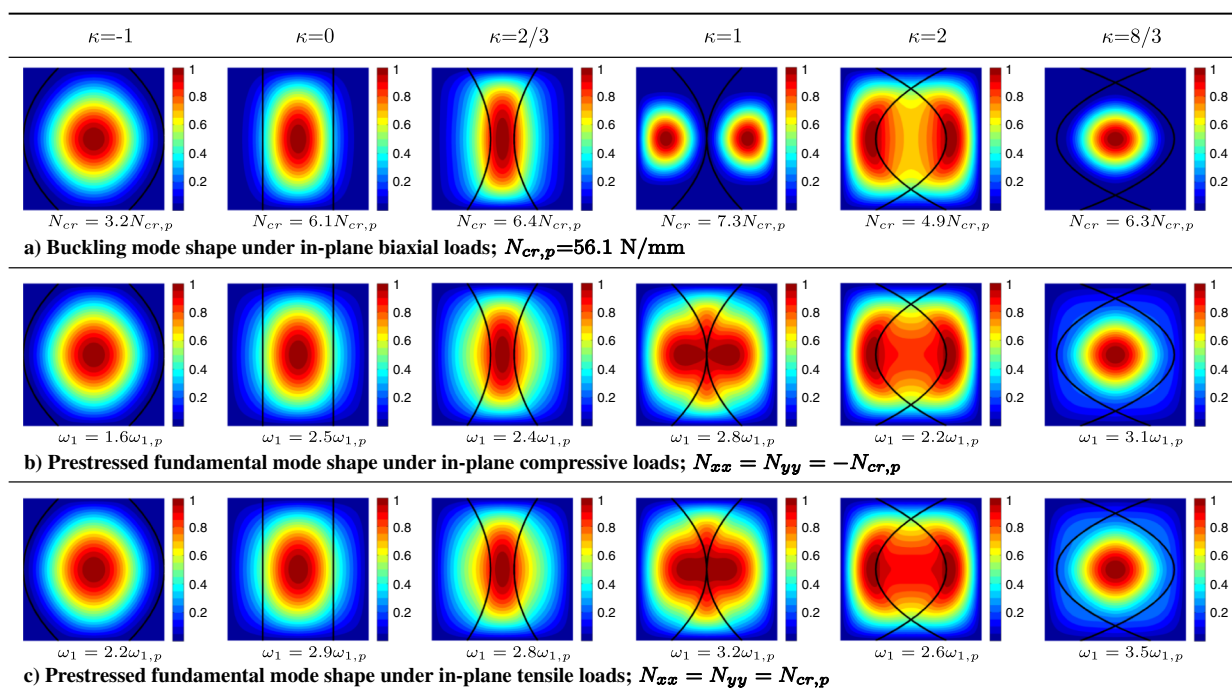


Fig. 14 Variation of the buckling mode shape and prestressed vibration mode shape with the stiffener geometric curvature under in-plane biaxial loads;  $\omega_{1,p} = 346.7$  rad/s.

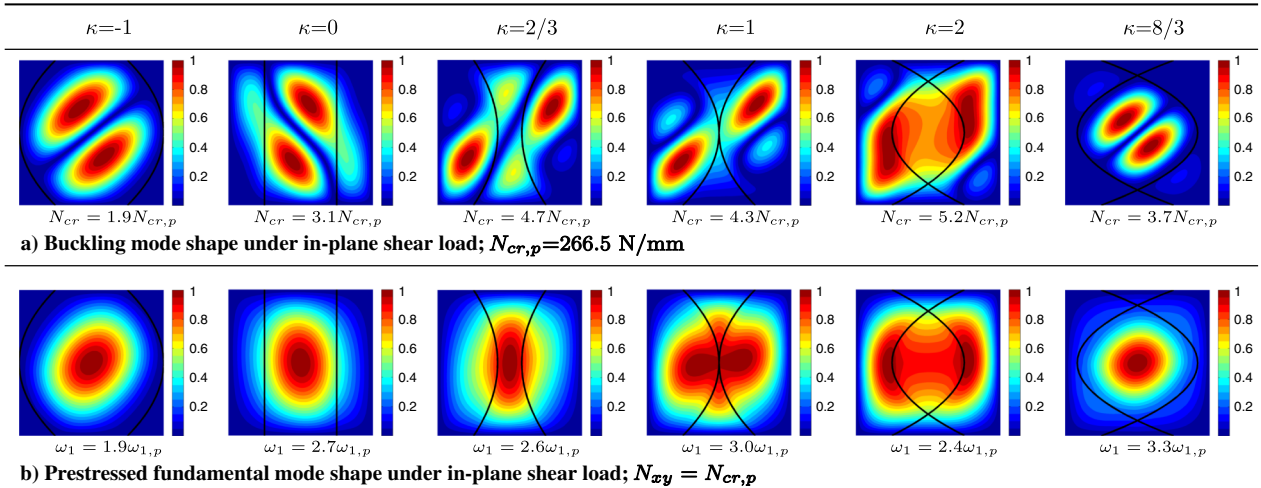


Fig. 15 Variation of the buckling mode shape and prestressed vibration mode shape with the stiffener geometric curvature under in-plane shear load;  $\omega_{1,p} = 346.7 \text{ rad/s}$ .

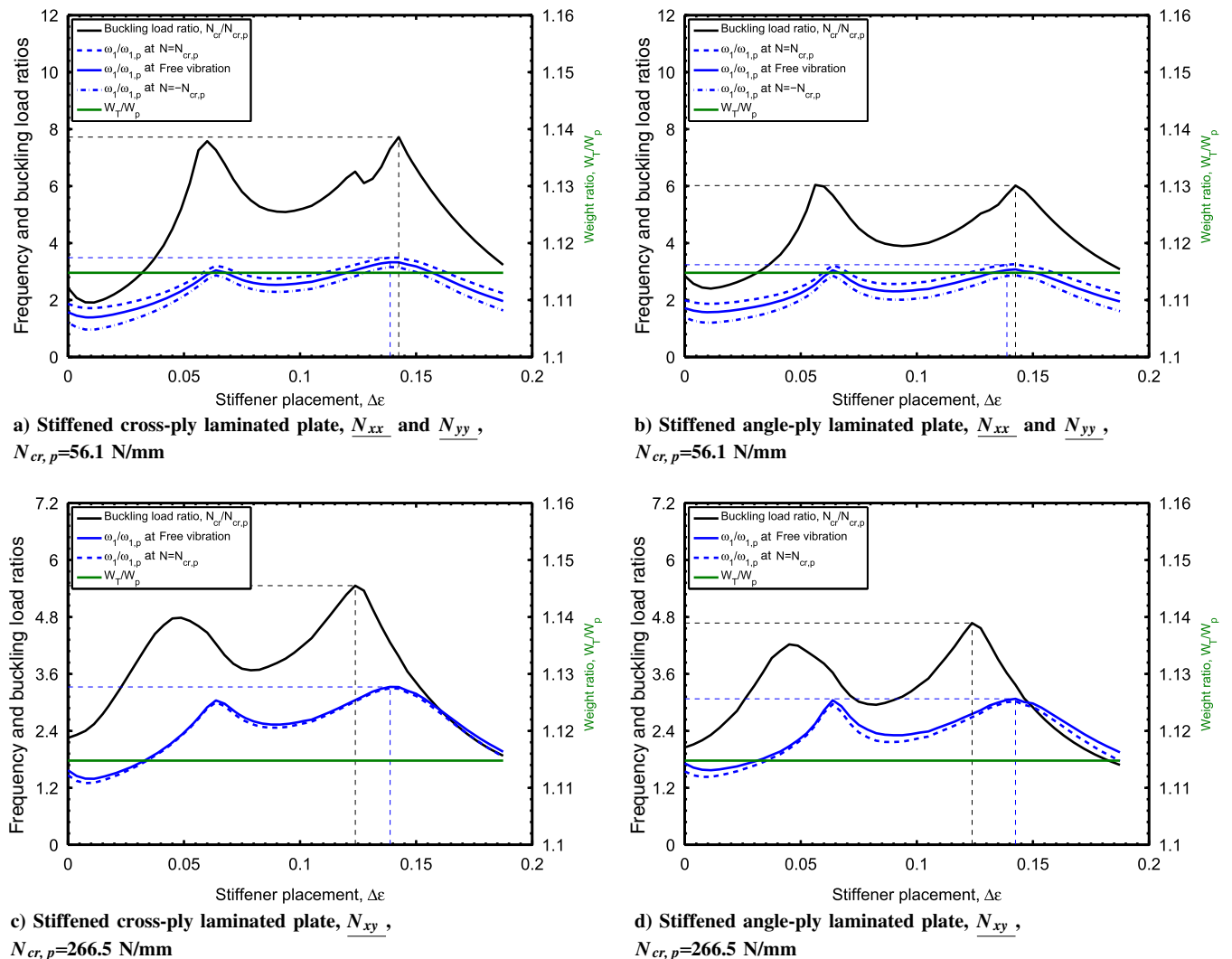


Fig. 16 Variation of the buckling load and the prestressed fundamental frequency with the stiffener placement;  $\omega_{1,p} = 346.7 \text{ rad/s}$ .

The variations of the prestressed vibration mode shape with the stiffener placement are shown in Figs. 17 and 18. As expected, the change in the mode shapes with the stiffener placement causes discontinuous changes in both the buckling load and the prestressed vibration mode frequency with the stiffener placement.

### 3. Influence of Stiffener Depth Ratio on Panel's Prestressed Vibration Responses

Figure 19 shows the variation of the buckling load and the fundamental frequency with the stiffener depth ratio  $h_s/b_s$  for the stiffened composite panel in the presence of in-plane biaxial and shear loads. The stiffener placement and the stiffener geometric

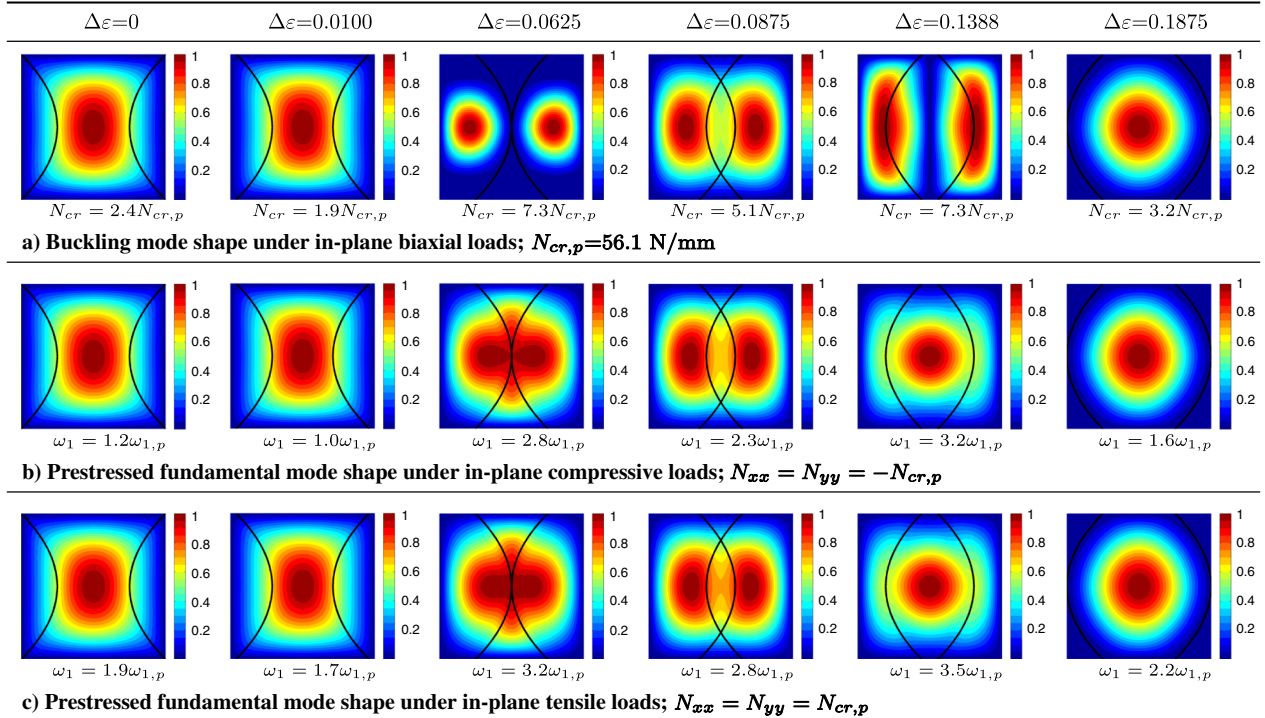


Fig. 17 Variation of the buckling mode shape and the prestressed fundamental mode shape with the stiffener placement under in-plane biaxial loads;  $\omega_{1,p} = 346.7 \text{ rad/s}$ .

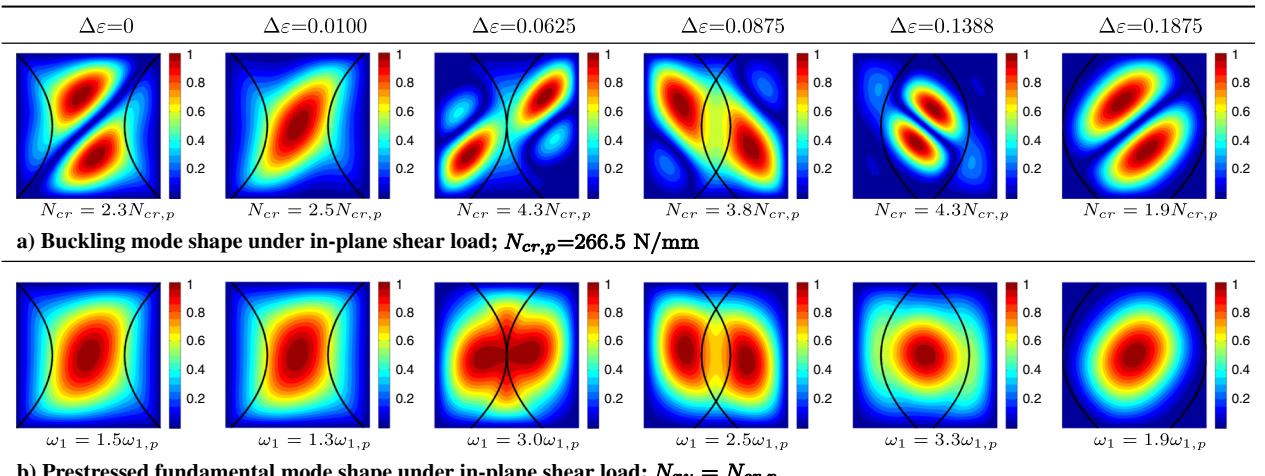


Fig. 18 Variation of the buckling mode shape and the prestressed fundamental mode shape with the stiffener placement under in-plane shear load;  $\omega_{1,p} = 346.7 \text{ rad/s}$ .

curvature for stiffener curve 1 are  $\Delta\varepsilon = 0.1388$  and  $\kappa = 1$ , respectively.

It is found that the prestressed vibration response can be further improved by changing the stiffener depth ratio in addition to tailoring the stiffener shape. For both laminated configurations, numerical results show that both the fundamental frequency and the buckling load increase significantly with the stiffener depth ratio  $h_s/b_s$ , but only up to a certain value, and then they become almost constant. This is because the increase in the stiffener depth ratio increases the stiffener equivalent bending stiffness, which could lead to the plate behaving as if it is simply supported along the stiffeners. Therefore, the buckling load remains almost constant with the stiffener depth ratio. The fundamental frequency reduces slightly with the stiffener depth ratio for both laminate configurations because the increase of the stiffener height leads to the increase of the values in both the mass and the rotational inertias. However, a further increase in the stiffener

depth ratio causes the buckling load to decrease significantly. This is because the increase in the stiffener depth ratio leads to the stiffener being much more flexible in the lateral direction. The stiffener's buckling occurs before the plate buckling. This phenomenon was explained by Timoshenko and Gere [30] and by Zhao and Kapania [22]. However, the fundamental frequency of the stiffened composite panel still reduces slightly with the stiffener depth ratio.

The variation in the buckling mode shape and the prestressed vibration mode shape with the stiffener depth ratio for the stiffened cross-ply laminated plate is examined, as shown in Figs. 20 and 21. For the two different load conditions, with the increase of the stiffener depth ratio, the mode shape transforms from a global mode to a local mode for both the vibration and buckling mode shapes. The buckling mode shapes for the plate at larger stiffener depth ratios reveal that the stiffeners buckle in the lateral direction. This explains that a further increase in the stiffener height leads to the

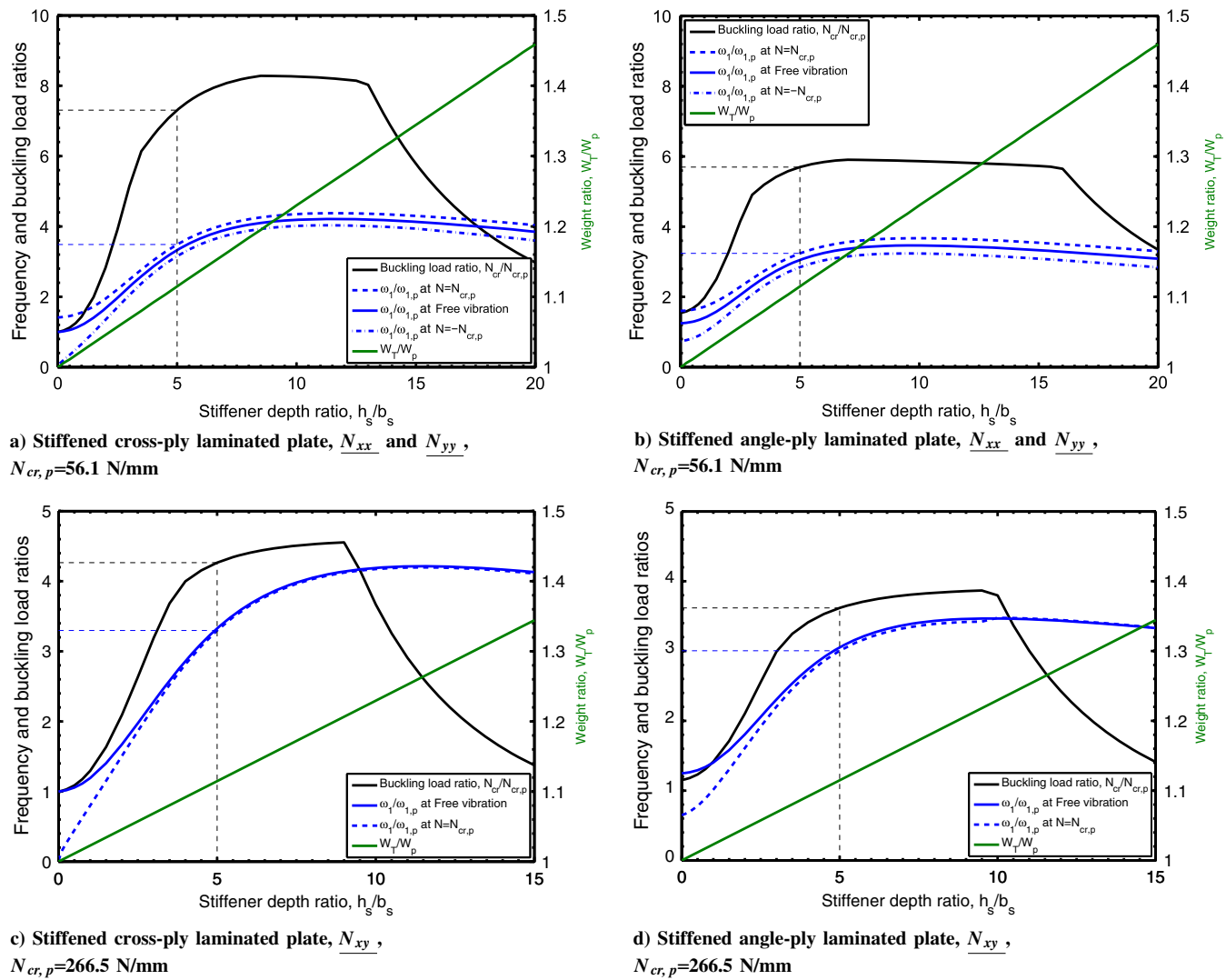


Fig. 19 Variation of the buckling load and the prestressed fundamental frequency with the stiffener depth ratio;  $\omega_{1,p} = 346.7$  rad/s.

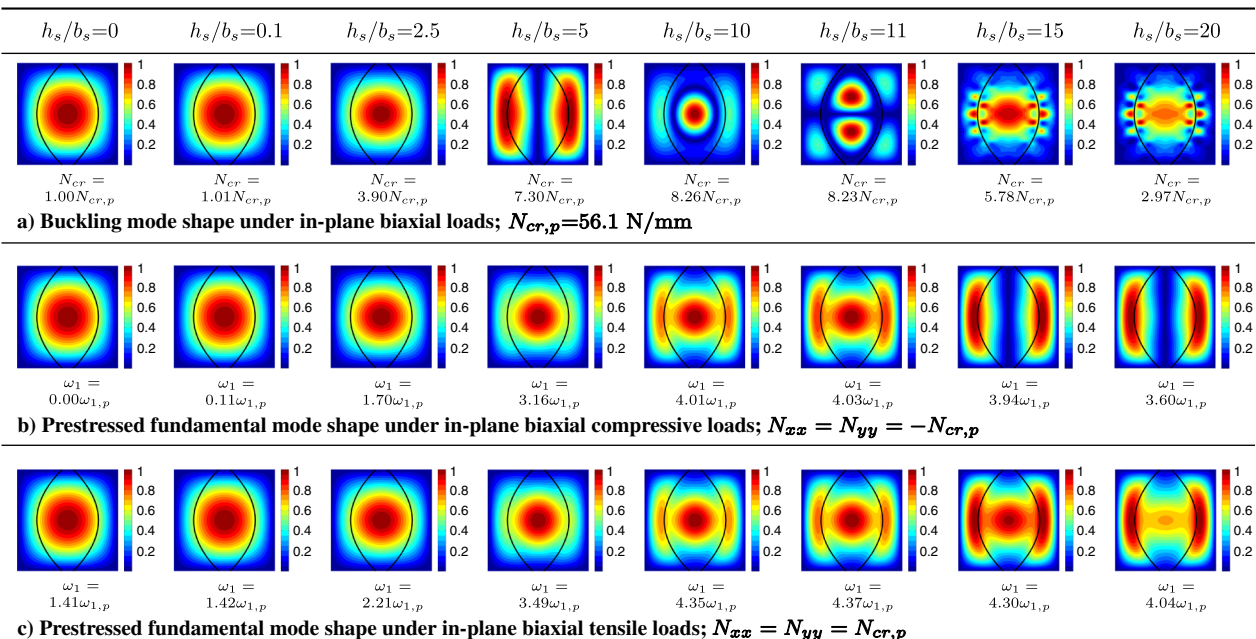


Fig. 20 Variation of the buckling mode shape and the prestressed fundamental mode shape with the stiffener depth ratio under in-plane biaxial loads;  $\omega_{1,p} = 346.7$  rad/s.

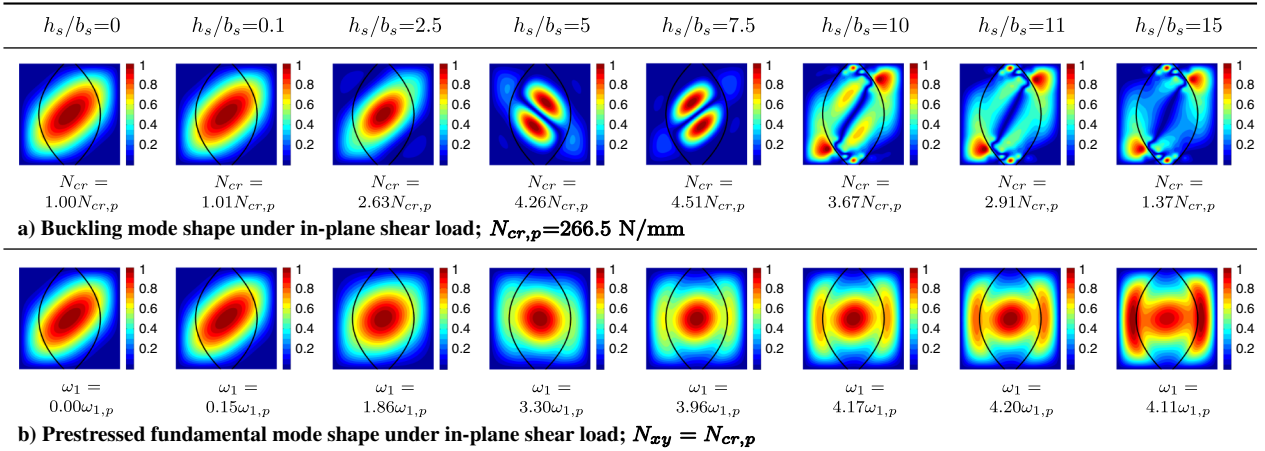


Fig. 21 Variation of the buckling mode shape and the prestressed fundamental mode shape with the stiffener depth ratio under in-plane shear load;  $\omega_{1,p} = 346.7 \text{ rad/s}$ .

stiffener buckling before the plate buckling, and it causes a significant reduction of the total critical buckling load with the stiffener depth ratio.

For the prestressed vibration mode shape corresponding to the fundamental frequency, the vibration mode shape morphs from a global mode to a local mode because of these near-simply supported boundary conditions along the stiffeners. The vibration mode shape for the stiffened plate at larger stiffener depth ratios is similar to the one for the plate with simply supported boundary conditions along the stiffeners, and it remains a local vibration mode shape with a further increase of the stiffener depth ratio. This explains why there is no dramatic decrease in the fundamental frequency of the prestressed plate with the stiffener depth ratio, as was the case for the buckling load.

For the stiffened composite plate subjected to the in-plane shear load at larger stiffener depth ratios within the given range, the fundamental frequency for the free vibration case and the prestressed vibration case are almost same. This is because the in-plane shear load has less effect on the fundamental frequency as compared to the in-plane normal load. For the stiffeners with the larger depth ratios within the given range, Figs. 20 and 21 both show that stiffener buckling does not affect the first vibration mode shape for the prestressed stiffened composite plate. It is also observed that the specific stiffness from the studied shaped stiffeners with the 0 deg laminated configurations improve both the buckling load and the fundamental frequency to a larger value for the cross-ply laminated plate than that for the angle-ply laminated plate.

#### IV. Conclusions

This paper studies the vibration response for a curvilinearly stiffened composite plate in the presence of in-plane biaxial and shear loads by using an efficient finite element approach. A first-order shear-deformable theory is used to model the responses for both the panel and the stiffeners. An eight-node isoparametric shell element and a three-node isoparametric beam element are used for modeling the panel and the stiffener, respectively. A linear approach is used to study the prestressed vibration response of the stiffened composite panel subjected to in-plane loads. The results obtained from the present method in the free vibration mode results compare well with those in the existing literature and those obtained by using MSC. NASTRAN. The influence of the stiffener shape, the laminate configuration, and the stiffener depth ratio on both the panel's free and prestressed vibration responses is studied.

Numerical results from the free vibration studies show that the stiffener shape changes the fundamental frequency significantly by changing the vibration mode shape. It is possible to tailor the stiffener shape to achieve the desired dynamic response by increasing the fundamental frequency and by changing the vibration mode shape with a lower or even no weight penalty. The stiffener depth ratio

increases the fundamental frequency significantly, but only up to a certain value. Any further increase in the stiffener depth ratio leads to the plate behaving as if it is simply supported along the stiffeners, and the increase in the values for the mass and rotational inertias due to the increased stiffener height leads to a slight decrease of the fundamental frequency with the stiffener depth ratio. Further improvement of the vibration response by using the laminated configuration can be achieved by adding the specific stiffness through tailoring of the stiffener shape.

Numerical results from the prestressed vibration studies show that the influences of the stiffener shape on the buckling load and the fundamental frequency are similar to each other. One can tailor the stiffener shape to improve the prestressed vibration response by simultaneously increasing the buckling load and the fundamental frequency to a large value. The influences of the stiffener depth ratio on the buckling load and the fundamental frequency are different from each other. Both the buckling load and the fundamental frequency increase significantly with the stiffener depth ratio up to a certain value. Any further increase in the stiffener depth ratio leads to the stiffener buckling before the plate buckling, whereas it causes the fundamental frequency to decrease slightly and leads the vibration mode shape to behave like the one for the plate with simply supported boundary conditions along the stiffeners.

The present parametric studies show that the laminate fiber ply orientation, the stiffener shape, and the stiffener depth ratio can all improve the prestressed vibration response significantly by increasing the value of the panel's fundamental frequency and the panel's buckling load with a lower or even no weight penalty. Along with the benefit of the present method in obviating the need for the repeated meshing when the stiffener shape changes arbitrarily in optimization, it is possible to integrate the present method to optimization framework EBF3PanelOpt [6,7] for the optimal stiffener shapes and the optimal laminated configurations in enhancing the dynamic performance.

#### Appendix A: Formulas for the Composite Panel

The kinematic relation for the generalized strain  $\boldsymbol{\epsilon}_p$  and the generalized displacement  $\boldsymbol{d}_p$  of the panel is

$$\boldsymbol{\epsilon}_p = \begin{pmatrix} \epsilon_x^0 \\ \epsilon_y^0 \\ \gamma_{xy}^0 \\ K_x^0 \\ K_y^0 \\ \gamma_{xy}^0 \\ \gamma_{xz}^0 \\ \gamma_{yz}^0 \end{pmatrix} = \begin{bmatrix} \frac{\partial}{\partial x} & 0 & 0 & 0 & 0 \\ 0 & \frac{\partial}{\partial y} & 0 & 0 & 0 \\ \frac{\partial}{\partial y} & \frac{\partial}{\partial x} & 0 & 0 & 0 \\ 0 & 0 & 0 & \frac{\partial}{\partial x} & 0 \\ 0 & 0 & 0 & 0 & \frac{\partial}{\partial y} \\ 0 & 0 & 0 & \frac{\partial}{\partial y} & \frac{\partial}{\partial x} \\ 0 & 0 & \frac{\partial}{\partial x} & 1 & 0 \\ 0 & 0 & \frac{\partial}{\partial y} & 0 & 1 \end{bmatrix} \begin{pmatrix} u_0 \\ v_0 \\ w_0 \\ \beta_x \\ \beta_y \end{pmatrix} = B_p \boldsymbol{d}_p$$

The matrix  $B_p^{\text{NL}}$  is [31]

$$B_p^{\text{NL}} = \begin{bmatrix} 0 & 0 & \frac{\partial}{\partial x} & 0 & 0 \\ 0 & 0 & \frac{\partial}{\partial y} & 0 & 0 \\ 0 & 0 & 0 & \frac{\partial}{\partial x} & 0 \\ 0 & 0 & 0 & \frac{\partial}{\partial y} & 0 \\ 0 & 0 & 0 & 0 & \frac{\partial}{\partial x} \\ 0 & 0 & 0 & 0 & \frac{\partial}{\partial y} \end{bmatrix}$$

The in-plane stress stiffness matrix  $\sigma_p$  for the composite panel is

$$\sigma_p = \text{diag} \left[ t_p \tau, \frac{1}{12} t_p^3 \tau, \frac{1}{12} t_p^3 \tau \right], \quad \tau = \begin{bmatrix} \sigma_x^0 & \sigma_{xy}^0 \\ \sigma_{xy}^0 & \sigma_y^0 \end{bmatrix}$$

The mass matrix  $m_p$  for the composite panel is expressed as

$$m_p = \rho_p \begin{bmatrix} t_p & 0 & 0 & 0 & 0 \\ 0 & t_p & 0 & 0 & 0 \\ 0 & 0 & t_p & 0 & 0 \\ 0 & 0 & 0 & \frac{1}{12} t_p^3 & 0 \\ 0 & 0 & 0 & 0 & \frac{1}{12} t_p^3 \end{bmatrix}$$

## Appendix B: Formulations for a Laminated Stiffener

The strain-displacement relation of the horizontal 3-D composite stiffener is assumed as [32]

$$\boldsymbol{\epsilon}_s = \begin{bmatrix} \epsilon_s^0 \\ \gamma_n^0 \\ \gamma_b^0 \\ \kappa_n^0 \\ \kappa_b^0 \end{bmatrix} = \begin{bmatrix} \frac{d}{dt} & \frac{1}{R} & 0 & 0 & 0 \\ -\frac{1}{R} & \frac{d}{dt} & 0 & 0 & 0 \\ 0 & 0 & \frac{d}{dt} & 1 & 0 \\ 0 & 0 & 0 & \frac{d}{dt} & \frac{1}{R} \\ 0 & 0 & 0 & -\frac{1}{R} & \frac{d}{dt} \end{bmatrix} \begin{bmatrix} u_t \\ v_n \\ w_b \\ \beta_t \\ \beta_n \end{bmatrix} = B_s \mathbf{d}_s \quad (\text{B1})$$

where  $R$  is the radius of curvature of the stiffener, which is calculated at the Gaussian integration point when using the finite element method, as shown in Appendix C.

For a stiffener that has symmetric layers perpendicular to the panels middle plane, constitutive matrix  $D_s$  is obtained for a 3-D composite beam with an open cross section:

$$D_s = \begin{bmatrix} h_s \bar{A}_{11} & 0 & h_s \bar{A}_{16} & h_s e \bar{A}_{11} & 0 \\ 0 & K h_s \bar{A}_{55} & 0 & 0 & K h_s e \bar{A}_{55} \\ h_s \bar{A}_{16} & 0 & h_s \bar{A}_{66} & h_s e \bar{A}_{16} & 0 \\ h_s e \bar{A}_{11} & 0 & h_s e \bar{A}_{16} & \left(\frac{h_s^3}{12} + h_s e^2\right) \bar{A}_{11} & 0 \\ 0 & K h_s e \bar{A}_{55} & 0 & 0 & GJ \end{bmatrix}$$

where

$$\bar{A}_{ij} = \sum_{k=1}^n \int_{z_k}^{z_{k+1}} \bar{Q}'_{ij} dz, \quad \bar{D}_{ij} = \sum_{k=1}^n \int_{z_k}^{z_{k+1}} z^2 \bar{Q}'_{ij} dz$$

and where  $\bar{Q}'_{ij}$  is the reduced stiffness matrix for the composite stiffener, which can be found in the work of Zhao and Kapania [22].

To account for the torsion of open cross sections based on the St. Venant theory of torsion, the equivalent torsional stiffness  $GJ$  in the preceding rigidity matrix  $D_s$  is used [20,25]:

$$GJ = \frac{Q_{55} + Q_{66}}{2} \frac{b_s^3 h_s}{3}$$

This simplification of the torsional stiffness is acceptable to study the influence of the stiffener shape on the plate's free vibration and prestressed vibration responses when the stiffener vibrates with the plate in the vibration mode shape corresponding to the fundamental frequency. On the other hand, when the plate deflects in antisymmetric modes about the stiffener, it is necessary to get an accurate expression for the stiffener torsional stiffness [33,34]. For simplicity, this paper uses the equivalent torsional stiffness for a parametric study.

The transformation matrix  $T_s$  transforms the stiffener displacements, described in the global coordinate system  $xyz$ ,  $\mathbf{d}_{sg}$ , to that described in the local coordinate system  $tnb$ ,  $\mathbf{d}_s$ :

$$T_s = \begin{bmatrix} \cos \alpha & \sin \alpha & 0 & 0 & 0 \\ -\sin \alpha & \cos \alpha & 0 & 0 & 0 \\ 0 & 0 & 1 & 0 & 0 \\ 0 & 0 & 0 & \cos \alpha & \sin \alpha \\ 0 & 0 & 0 & -\sin \alpha & \cos \alpha \end{bmatrix}$$

where  $\alpha$  is shown in Fig. 1b.

The expressions for  $B_s^{\text{NL}}$  and  $\sigma_s$  for the stiffener geometric stiffness are

$$B_s^{\text{NL}} = \begin{bmatrix} \frac{d}{dt} & 0 & 0 \\ 0 & \frac{d}{dt} & \frac{1}{R} \\ 0 & -\frac{1}{R} & \frac{d}{dt} \end{bmatrix}, \quad \sigma_s = \sigma_{tt} \begin{bmatrix} A_s & 0 & 0 \\ 0 & I_n & 0 \\ 0 & 0 & I_n \end{bmatrix}$$

The expression for the stiffener axial stress  $\sigma_{tt}$  can be found in [22]. The mass matrix  $m_s$  for the composite stiffener is expressed as

$$m_s = \rho_s \begin{bmatrix} A_s & 0 & 0 & A_s e & 0 \\ 0 & A_s & 0 & 0 & A_s e \\ 0 & 0 & A_s & 0 & 0 \\ A_s e & 0 & 0 & I_n & 0 \\ 0 & A_s e & 0 & 0 & I_n + I_b \end{bmatrix}$$

where  $I_n = (1/12)b_s h_s^3 + e^2 A_s$  and  $I_b = (1/12)b_s^3 h_s$  are the second moments of area around the  $n$  and  $b$  axes, respectively.

## Appendix C: Finite Element Formulation

The Jacobian matrix  $J_p$  for the eight-node shell element is

$$\left\{ \frac{\partial}{\partial x} \right\} = J_p^{-1} \left\{ \frac{\partial}{\partial \xi} \right\}, \quad J_p = \begin{bmatrix} \sum_{i=1}^8 \frac{\partial N_{p,i}}{\partial \xi} x_i & \sum_{i=1}^8 \frac{\partial N_{p,i}}{\partial \xi} y_i \\ \sum_{i=1}^8 \frac{\partial N_{p,i}}{\partial \eta} x_i & \sum_{i=1}^8 \frac{\partial N_{p,i}}{\partial \eta} y_i \end{bmatrix}$$

The Jacobian  $J_s$  for the three-node quadratic beam element is

$$J_s = \left[ \left( \sum_{i=1}^3 N_{s,i} x_i \right)^2 + \left( \sum_{i=1}^3 N_{s,i} y_i \right)^2 \right]^{1/2}$$

Curvature  $1/R$  in Eq. (B1) for the curved stiffener is expressed as [32]

$$\frac{1}{R} = \left( \sum_{i=1}^3 \frac{dN_{s,i}}{d\xi} y_i \sum_{i=1}^3 \frac{d^2 N_{s,i}}{d\xi^2} x_i - \sum_{i=1}^3 \frac{dN_{s,i}}{d\xi} x_i \sum_{i=1}^3 \frac{d^2 N_{s,i}}{d\xi^2} y_i \right) / (\det J_s)^3$$

## Acknowledgments

The authors would like to thank the reviewers for their highly valuable comments and suggestions.

## References

- [1] Renton, W. J., Olcott, D., Roeseler, W., Batzer, R., Baron, W., and Velicki, A., "Future of Flight Vehicle Structures (2002 to 2023)," *Journal of Aircraft*, Vol. 41, No. 5, 2004, pp. 986–998.  
doi:10.2514/1.4039
- [2] Forster, E., Clay, S., Holzwarth, R., Pratt, D., and Paul, D., "Flight Vehicle Composite Structures," *26th Congress of International Council of the Aeronautical Sciences (ICAS)*, AIAA Paper 2008-8976, 2008.
- [3] Jegley, D., and Velicki, A., "Status of Advanced Stitched Unitized Composite Aircraft Structures," *51st AIAA Aerospace Sciences Meeting Including the New Horizons Forum and Aerospace Exposition*, AIAA Paper 2013-0410, 2013.
- [4] Kapania, R. K., Li, J., and Kapoor, H., "Optimal Design of Unitized Panels with Curvilinear Stiffeners," *AIAA 5th ATIO and the AIAA 16th Lighter-than-Air Systems Technology Conference and Balloon Systems Conference*, AIAA Paper 2005-7482, 2005.
- [5] Locatelli, D., Mulani, S. B., and Kapania, R. K., "Wing-Box Weight Optimization Using Curvilinear Spars and Ribs (SpaRibs)," *Journal of Aircraft*, Vol. 48, No. 5, 2011, pp. 1671–1684.  
doi:10.2514/1.C031336
- [6] Mulani, S. B., Slemp, W. C., and Kapania, R. K., "EBF3PanelOpt: An Optimization Framework for Curvilinear Blade-Stiffened Panels," *Thin-Walled Structures*, Vol. 63, 2013, pp. 13–26.  
doi:10.1016/j.tws.2012.09.008
- [7] Liu, Q., Jrad, M., Mulani, S. B., and Kapania, R. K., "Global/Local Optimization of Aircraft Wing Using Parallel Processing," *AIAA Journal*, June 2016.  
doi:10.2514/1.J054499
- [8] Kapania, R. K., and Raciti, S., "Recent Advances in Analysis of Laminated Beams and Plates. Part I-Shear Effects and Buckling," *AIAA Journal*, Vol. 27, No. 7, 1989, pp. 923–935.  
doi:10.2514/3.10202
- [9] Zhang, Y., and Yang, C., "Recent Developments in Finite Element Analysis for Laminated Composite Plates," *Composite Structures*, Vol. 88, No. 1, 2009, pp. 147–157.  
doi:10.1016/j.compstruct.2008.02.014
- [10] Reddy, J. N., and Khdeir, A., "Buckling and Vibration of Laminated Composite Plates Using Various Plate Theories," *AIAA Journal*, Vol. 27, No. 12, 1989, pp. 1808–1817.  
doi:10.2514/3.10338
- [11] Carrera, E., Nali, P., Lecca, S., and Soave, M., "Effects of In-Plane Loading on Vibration of Composite Plates," *Shock and Vibration*, Vol. 19, No. 4, 2012, pp. 619–634.  
doi:10.1155/2012/318931
- [12] Lee, D. M., and Lee, I., "Vibration Analysis of Anisotropic Plates with Eccentric Stiffeners," *Computers and Structures*, Vol. 57, No. 1, 1995, pp. 99–105.  
doi:10.1016/0045-7949(94)00593-R
- [13] Rikards, R., Chate, A., and Ozolinsh, O., "Analysis for Buckling and Vibrations of Composite Stiffened Shells and Plates," *Composite Structures*, Vol. 51, No. 4, 2001, pp. 361–370.  
doi:10.1016/S0263-8223(00)00151-3
- [14] Patel, S., Datta, P., and Sheikh, A., "Buckling and Dynamic Instability Analysis of Stiffened Shell Panels," *Thin-Walled Structures*, Vol. 44, No. 3, 2006, pp. 321–333.  
doi:10.1016/j.tws.2006.03.004
- [15] Mukherjee, A., and Mukhopadhyay, M., "Finite Element Free Vibration of Eccentrically Stiffened Plates," *Computers and Structures*, Vol. 30, No. 6, 1988, pp. 1303–1317.  
doi:10.1016/0045-7949(88)90195-2
- [16] Biswal, K., and Ghosh, A., "Finite Element Analysis for Stiffened Laminated Plates Using Higher Order Shear Deformation Theory," *Computers and Structures*, Vol. 53, No. 1, 1994, pp. 161–171.  
doi:10.1016/0045-7949(94)90139-2
- [17] Ghosh, A. K., and Biswal, K., "Free-Vibration Analysis of Stiffened Laminated Plates Using Higher-Order Shear Deformation Theory," *Finite Elements in Analysis and Design*, Vol. 22, No. 2, 1996, pp. 143–161.  
doi:10.1016/0168-874X(95)00051-T
- [18] Kumar, Y. S., and Mukhopadhyay, M., "A New Triangular Stiffened Plate Element for Laminate Analysis," *Composites Science and Technology*, Vol. 60, No. 6, 2000, pp. 935–943.  
doi:10.1016/S0266-3538(99)00190-6
- [19] Kumar, Y. S., and Srivastava, A., "First Ply Failure Analysis of Laminated Stiffened Plates," *Composite Structures*, Vol. 60, No. 3, 2003, pp. 307–315.  
doi:10.1016/S0263-8223(02)00350-1
- [20] Kumar, Y. S., and Mukhopadhyay, M., "A New Finite Element for Buckling Analysis of Laminated Stiffened Plates," *Composite Structures*, Vol. 46, No. 4, 1999, pp. 321–331.  
doi:10.1016/S0263-8223(99)00059-8
- [21] Shi, P., Kapania, R. K., and Dong, C., "Vibration and Buckling Analysis of Curvilinearly Stiffened Plates Using Finite Element Method," *AIAA Journal*, Vol. 53, No. 5, 2015, pp. 1319–1335.  
doi:10.2514/1.J053358
- [22] Zhao, W., and Kapania, R. K., "Buckling Analysis of Unitized Curvilinearly Stiffened Composite Panels," *Composite Structures*, Vol. 135, Jan. 2016, pp. 365–382.  
doi:10.1016/j.compstruct.2015.09.041
- [23] Prusty, B. G., and Satsangi, S., "Analysis of Stiffened Shell for Ships and Ocean Structures by Finite Element Method," *Ocean Engineering*, Vol. 28, No. 6, 2001, pp. 621–638.  
doi:10.1016/S0029-8018(00)00021-4
- [24] Prusty, B., and Satsangi, S., "Finite Element Transient Dynamic Analysis of Laminated Stiffened Shells," *Journal of Sound and Vibration*, Vol. 248, No. 2, 2001, pp. 215–233.  
doi:10.1006/jsvi.2001.3678
- [25] Kumar, Y. S., and Mukhopadhyay, M., "Transient Response Analysis of Laminated Stiffened Plates," *Composite Structures*, Vol. 58, No. 1, 2002, pp. 97–107.  
doi:10.1016/S0263-8223(02)00036-3
- [26] Zhao, W., and Kapania, R. K., "Vibrational Analysis of Unitized Curvilinearly Stiffened Composite Panels Subjected to In-Plane Loads," *57th AIAA/ASCE/AHS/ASC Structures, Structural Dynamics, and Materials Conference*, AIAA Paper 2016-1500, 2016.
- [27] Reddy, J. N., *Mechanics of Laminated Composite Plates: Theory and Analysis*, 2nd ed., CRC Press, Boca Raton, FL, 2004, pp. 132–142.
- [28] Onate, E., *Structural Analysis with the Finite Element Method. Linear Statics*, Vol. 2, *Beams, Plates and Shells*, Springer Science and Business Media, New York, 2013, pp. 58–62.
- [29] Tamjiani, A. Y., and Kapania, R. K., "Vibration of Plate with Curvilinear Stiffeners Using Mesh-Free Method," *AIAA Journal*, Vol. 48, No. 8, 2010, pp. 1569–1581.  
doi:10.2514/1.43082
- [30] Timoshenko, S. P., and Gere, J. M., *Theory of Elastic Stability*, McGraw-Hill, New York, 1963, pp. 225–228.
- [31] Tamjiani, A. Y., and Kapania, R. K., "Buckling and Static Analysis of Curvilinearly Stiffened Plates Using Mesh-Free Method," *AIAA Journal*, Vol. 48, No. 12, 2010, pp. 2739–2751.  
doi:10.2514/1.43917
- [32] Martini, L., and Vitaliani, R., "On the Polynomial Convergent Formulation of a  $C_0$  Isoparametric Skew Beam Element," *Computers and Structures*, Vol. 29, No. 3, 1988, pp. 437–449.  
doi:10.1016/0045-7949(88)90396-3
- [33] Nemeth, M. P., "A Treatise on Equivalent-Plate Stiffnesses for Stiffened Laminated-Composite Plates and Plate-Like Lattices," NASA Rept. TP-2011-216882, 2011.
- [34] Coburn, B. H., Wu, Z., and Weaver, P. M., "Buckling Analysis of Stiffened Variable Angle Tow Panels," *Composite Structures*, Vol. 111, May 2014, pp. 259–270.  
doi:10.1016/j.compstruct.2013.12.029

P. Weaver  
Associate Editor